"Study of Temperature Anisotropy and Kappa Distribution Impacts on EMIC Waves in Multi-Species Magnetized Plasma"

Rahul Bhaisaniya[1] and Ganpat Ahirwar[2]

[1]Assistant Professor,Govt PG college Rajgarh, MP,India

[2]Assistant Professor ,School of Studies in Physics,Vikram University Ujjain (M.P.)India

[1]EMail :rahulbhaisaniya@gmail.com

[1]EMail :ganpat.physics@gmail.com

Abstract:- This research investigates the impact of temperature anisotropy on Electromagnetic ion cyclotron (EMIC) waves in a multi-ion magneto-plasma environment composed of H^+, He^+, and O^+ ions, with a particular emphasis on the role of the Kappa distribution function. The study delves into how variations in temperature anisotropy influence the behavior and properties of EMIC wave propagation, considering the complex interplay between anisotropic thermal effects and the non-Maxwellian Kappa distribution. Through a comprehensive analysis involving theoretical modeling and numerical simulations, the research elucidates how these factors alter wave dispersion relations, growth rates, and spatial structures of EMIC waves. The results reveal significant deviations from classical Maxwellian predictions, highlighting the necessity to incorporate Kappa distributions for accurate descriptions of wave behavior in realistic plasma conditions. This enhanced understanding has broader implications for space physics, astrophysical phenomena, and laboratory plasma experiments, where non-equilibrium conditions and multiple ion species are prevalent. The results are analyzed in the context of space plasma parameters relevant region within Earth's magnetosphere.

1. Introduction

EMIC waves are transverse, low-frequency (below the proton cyclotron frequency) waves typically in the range of 0.1–5 Hz, which manifest as Pc1–Pc2 pulsations on the ground. These waves are primarily generated in the equatorial region of Earth's magnetosphere and propagate along magnetic field lines as left-handed, circularly polarized waves, guided toward the ionosphere (Sugiyama et al., 1999). Their oblique propagation characteristics and interactions with anisotropic plasma distributions have been extensively studied (Cattaert, Hellberg & Mace, 2007). Experimental evidence for naturally occurring ion cyclotron instabilities has been comprehensively summarized by Cornwall (1965).

Formatted: Numbered + Level: 1 + Numbering Style: 1, 2, 3, … + Start at: 1 + Alignment: Left + Aligned at: 0.32 cm + Indent at: 0.95 cm

Formatted: Line spacing: 1.5 lines

In the auroral acceleration region, located at magnetic latitudes of approximately ±70° and altitudes above 4000 km, large-amplitude electric field structures have been observed. The parallel electric fields in this region, concentrated around 6000 km altitude, are strongly associated with field-aligned currents (Yan et al., 2008). This region is characterized by low plasma beta (β) and cold plasma environments, making it a critical zone for understanding wave-particle interactions. EMIC waves play a vital role in space plasma physics, particularly in the Earth's magnetosphere, where they influence particle dynamics, energy transfer, and plasma stability (Gary & Lee , 1994). These waves interact with energetic particles, drive pitch-angle scattering, and facilitate the heating of ion populations, making them a cornerstone of magnetospheric studies (Kennel & Petschek, 1966; Chen & Hasegawa, 1974). The triggered emissions associated with EMIC waves have been observed in satellite data and analyzed in theoretical studies (Omura et al., 2010).

The propagation of EMIC waves at frequencies near the ion cyclotron frequency has been extensively studied under the assumption of Maxwellian velocity distributions, which describe thermal plasmas. However, real plasma environments, especially in the magnetosphere, often deviate from thermal equilibrium due to the presence of suprathermal particles (Sugiyama et al., 2015). The Kappa distribution function (Vasyliunas, 1968) is widely used to describe such non-thermal plasma environments. It is characterized by the parameter , which governs the extent of high-energy tails in the particle velocity distribution. Lower kappa values correspond to stronger deviations from thermal equilibrium, making the Kappa distribution particularly relevant for modeling space plasmas where suprathermal particles dominate (Pierrard & Lazar, 2010). A generalized plasma dispersion function for kappa-Maxwellian velocity distributions has been formulated to describe the wave behavior in these conditions (Hellberg & Mace, 2002).

Temperature anisotropy, where the temperature differs along directions parallel and perpendicular to the magnetic field, further adds complexity to the plasma environment. This anisotropy significantly influences wave growth, dispersion characteristics, and stability. In anisotropic magneto-plasma, enhanced perpendicular temperatures relative to the parallel component can amplify EMIC wave growth and alter dispersion relations compared to isotropic conditions (Hellinger & Matsumoto, 2000). When coupled with the Kappa distribution, temperature anisotropy introduces novel wave behaviors and complexities that deviate significantly from Maxwellian models (Lazar et al., 2006). The effects of temperature anisotropy on wave growth have been observed in bi-Kappa distributed plasmas, where deviations from Maxwellian distributions further modify wave dispersion (Lazar,

2012). The influence of suprathermal protons on EMIC wave instability thresholds has also been examined in kappa-distributed plasmas (Xiao et al., 2007).

Despite extensive research on plasma instabilities, a significant gap remains in understanding how temperature anisotropy and Kappa distributions simultaneously affect EMIC wave dynamics. The novelty of this study lies in addressing this critical gap by examining how temperature anisotropy influences the dispersion relations, growth rates, and spatial structures of EMIC waves in a multi-ion magneto-plasma under the influence of the Kappa distribution. Unlike earlier works that focused predominantly on single-ion plasmas or isotropic temperature assumptions, this research emphasizes the role of multi-ion plasma composition (e.g., H^+, He^+, O^+) and varying kappa values, which are particularly relevant for understanding wave-particle interactions near the plasmapause and auroral acceleration regions. Previous studies have demonstrated how EMIC waves grow and dampen under different conditions, including oblique propagation and multi-ion species effects (Xue, Thorne, & Summers, 1996a, 1996b).

This study investigates the combined effects of temperature anisotropy and the Kappa distribution on EMIC wave dynamics, focusing on perpendicular and parallel resonant energies, growth rate, and growth length in a multi-ion plasma environment. By incorporating these complex plasma conditions, we aim to advance the accuracy of space plasma models, particularly within the magnetosphere, where these factors are paramount. The findings hold significant implications for space weather forecasting and the mitigation of associated disturbances, given EMIC waves influence on particle precipitation, ion heating, and geomagnetic activity. By rigorously quantifying the individual and combined impact of the Kappa distribution and temperature anisotropy, this research provides deeper insights into EMIC wave behaviour, enhancing our understanding of wave-particle interactions in space plasmas thereby improving the interpretation of satellite data.

~~Electromagnetic ion cyclotron (EMIC) waves are transverse, low frequency (below the proton cyclotron frequency) waves in the range of 0.1-5Hz are seen on the ground as pc1-pc2 pulsations. Electromagnetic ion cyclotron waves generated in In the equatorial region of Earth's magnetosphere, left handed circularly polarized waves propagate along magnetic field lines, guided towards the ionosphere[15]. Experiment evidence for naturally occurring ion cyclotron instability has been summarized by Cornwall. The auroral acceleration region present about the earth at magnetic latitudes of about ±70 and at altitude between a typically above 4000km. In this region, large amplitude electric field structure has been observed . According to Yan et al., the auroral acceleration region can be approximated as a low β, cold~~

plasma environment. The parallel electric fields are generally observed to be concentrated around 6000 km altitude, a zone known as the auroral acceleration region. Although the exact nature of parallel electric fields remains debated, most researchers link them to the field-aligned currents present in the auroral region[24].

Electromagnetic ion cyclotron (EMIC) waves are significant in space plasma physics, particularly within the Earth's magnetosphere, where they influence particle dynamics, energy transfer, and overall plasma behaviour (Anderson & Williams, 1999; Kennel & Petschek, 1966). These waves propagate at frequencies near the ion cyclotron frequency and are crucial for understanding various plasma processes, including wave-particle interactions and the heating of ion populations (Chen & Hasegawa, 1974).

Traditionally, studies of EMIC waves have employed the Maxwellian distribution to describe particle velocities in plasmas. However, the Kappa distribution function, characterized by its parameter kappa, provides a more nuanced representation of particle velocity distributions, especially in environments where non-thermal or suprathermal particles are prevalent (Pierrard & Lazar, 2010). This distribution function better accommodates the high-energy tails observed in many astrophysical and space plasma contexts, making it a valuable tool for accurately modelling wave phenomena in these settings (Vasyliunas, 1968).

Temperature anisotropy, where the temperature varies along different spatial directions, further complicates the plasma environment. Anisotropic temperature conditions can significantly affect wave propagation, altering dispersion relations, growth rates, and wave stability (Hellinger & Matsumoto, 2000). For instance, in a magneto-plasma with anisotropic temperatures, the perpendicular and parallel temperatures relative to the magnetic field can lead to enhanced wave growth and modified dispersion characteristics compared to isotropic conditions (Zhang & Chen, 2003).

When combined with a Kappa distribution, the effects of temperature anisotropy introduce additional complexities. The interaction between the Kappa distribution and temperature anisotropy can lead to novel wave behaviors that deviate from those predicted by Maxwellian distributions alone (Del Sarto, Pegoraro, & D'Angelo, 2011; Scholer, 1988). This interaction can impact various plasma parameters, including wave amplitude, frequency, and spatial structure, thereby influencing the overall dynamics of the plasma system.

~~Despite the significance of these factors, the combined effects of temperature anisotropy and Kappa distribution on EMIC waves remain underexplored. Understanding these interactions is essential for improving theoretical models and practical applications in space and laboratory plasmas, where complex conditions often prevail. This study aims to bridge this gap by examining how temperature anisotropy affects EMIC wave characteristics in a multi-ion magneto-plasma environment under the influence of a Kappa distribution function. By integrating theoretical analysis with numerical simulations, this research seeks to provide a comprehensive understanding of wave dynamics in such complex plasma systems.~~

2. Basic trajectories

Considering the trajectory of a charged particle in the presence of EMIC waves, various properties have been derived for different Kappa distribution indices (Rana et al., 2021). Given that the wave propagates along the z-axis in the direction of the background magnetic field, the left-handed circularly polarized EMIC wave in a cold magnetized plasma with angular frequency ω can be expressed as follows ~~Consider the path of the particle in the presence of EMIC waves ,various properties are derived for different kappa distribution index k_p (Rana *et.al 2021)*[1].~~

~~Given that the wave travels along the z-axis in the specified direction of the magnetic field, the left-handed circularly polarized EMIC wave in a cold magnetized plasma with angular frequency ω is defined as follows~~

$$B_x = \cos(k_{I\Pi}z - \omega t) \quad (1)$$

$$B_y = \sin(k_{I\Pi}z - \omega t) \quad (2)$$

When the system moves with the wave, the electric field reduces to zero. (Rana et al., 2021)

$$B = B_x \cos(k_{I\Pi}z)\, x + B_y \sin(k_{I\Pi}z)\, y \quad (3)$$

Where the following conditions apply

$$Z^{wave} = Z^{lab} - \left(\frac{\omega}{k_{I\Pi l}}\right) t \quad (4)$$

$$V^{wave} = V^{lab} - \left(\frac{\omega}{k}\right) t \quad (5)$$

Formatted: Numbered + Level: 1 + Numbering Style: 1, 2, 3, … + Start at: 1 + Alignment: Left + Aligned at: 0.32 cm + Indent at: 0.95 cm

Formatted: Justified

Formatted: Font: (Default) Times New Roman, Complex Script Font: Times New Roman

As $\frac{ck}{\omega} \gg 1$, The magnetic field amplitude is considered identical.~~–~~Z^{wave}: Position of the particle in the wave frame of reference.

V^{wave}: Position of the particle in the laboratory frame of reference. Thus, the equation of ion motion in the wave is given as

~~Thus, the equation of ion motion in the wave is given as~~

$$\frac{d\boldsymbol{v_l}}{\boldsymbol{dt}} = \frac{q_l}{m_l c}[(V_l \times B_O) + (V_l \times B)] \quad (6)$$

We use cylindrical coordinates in velocity space as follows

$$v_{lx} = V_{\perp l} \cos\phi \quad (7)$$

$$v_{ly} = V_{\perp 1} \sin\phi \quad (8)$$

$$v_{\perp lz} = V_{\Pi l} \quad (9)$$

The equation of motion is written as

$$\frac{dV_{\perp l}}{dt} = -V_{\Pi l}\Omega_l \sin(k_{\Pi} z - \phi) \quad (10)$$

$$\mathrm{V}_{\perp 1} = \mathrm{V}_{\Pi \mathrm{lo}} + \delta \mathrm{V}_{\perp 1} \quad (11)$$

$$\mathrm{V}_{\Pi \mathrm{l}} = \mathrm{V}_{\Pi \mathrm{lo}} + \delta \mathrm{V}_{\Pi \mathrm{l}} \quad (12)$$

Where $\mathrm{V}_{\Pi \mathrm{i}}$ initial values at t=0, Substituting eq. (1) to (5) in eq. (11~~6~~) and (12~~7~~) we find the following equations of t~~T~~he alterations in multi-ion velocities in the context of an EMIC wave are provided as(Rana et al., 2021),

$$\delta \mathrm{V}_{\perp l} = \frac{\left[h\Omega_{H^+}\left(V_{\Pi H^+} - \frac{\omega}{K_{\Pi}}\right)\right]}{\left[k_{\Pi} V_{\Pi H^+ o} - (\omega - \Omega_{H^+})\right]} \times \left[\cos(k_{\Pi l}\mathrm{z} - \omega \mathrm{t} - \Psi) - \varepsilon \cos(k_{\Pi l}\mathrm{z} - \omega \mathrm{t} - \Psi - \left(k_{\Pi l} V_{\Pi H^+ o} - (\omega - \Omega_{H^+})\right)\mathrm{t}\right] + \frac{\left[h\Omega_{He^+}\left(V_{\Pi He^+} - \frac{\omega}{K_{\Pi}}\right)\right]}{\left[k_{\Pi} V_{\Pi He^+ o} - (\omega - \Omega_{He^+})\right]} \times \left[\cos(k_{\Pi l}\mathrm{z} - \omega \mathrm{t} - \Psi) - \varepsilon \cos(k_{\Pi l}\mathrm{z} - \omega \mathrm{t} - \Psi - \left(k_{\Pi l} V_{\Pi He^+ o} - (\omega - \Omega_{He^+})\right)\mathrm{t}\right] + \frac{\left[h\Omega_{O^+}\left(V_{\Pi O^+} - \frac{\omega}{K_{\Pi}}\right)\right]}{\left[k_{\Pi} V_{\Pi O^+ o} - (\omega - \Omega_{O^+})\right]} \times \left[\cos(k_{\Pi l}\mathrm{z} - \omega \mathrm{t} - \Psi) - \varepsilon \cos(k_{\Pi l}\mathrm{z} - \omega \mathrm{t} - \Psi - \left(k_{\Pi l} V_{\Pi O^+ o} - (\omega - \Omega_{O^+})\right)\mathrm{t}\right] \quad (13)$$

Formatted: Justified

Formatted: Right

Formatted: Justified

$$\delta V_{\Pi l} = \frac{-hV_{\perp o}\Omega_{H^+}}{[k_\Pi V_{\Pi H^+ o} - (\omega - \Omega_{H^+})]} \times [\cos(k_\Pi z - \omega t - \Psi) - \varepsilon \cos(k_\Pi z - \omega t - \Psi - (k_\Pi V_{\Pi H^+ o} - (\omega - \Omega_l))t] + \frac{-hV_{\perp o}\Omega_{H^+}}{[k_\Pi V_{\Pi He^+ o} - (\omega - \Omega_{He^+})]} \times [\cos(k_\Pi z - \omega t - \Psi) - \varepsilon \cos(k_\Pi z - \omega t - \Psi - (k_\Pi V_{\Pi He^+ o} - (\omega - \Omega_l))t] + \frac{-hV_{\perp o}\Omega_{O^+}}{[k_\Pi V_{\Pi O^+ o} - (\omega - \Omega_{O^+})]} \times [\cos(k_\Pi z - \omega t - \Psi) - \varepsilon \cos(k_\Pi z - \omega t - \Psi - (k_\Pi V_{\Pi O^+ o} - (\omega - \Omega_l))t] \quad (14)$$

Where $z = z_0 + V_\Pi t$ and $\psi = \psi_0 - \omega t$ and where ε=0 for non-resonant particles and ε=1 for resonant particles $h = \frac{B}{B_0}$.where $l = H^+/He^+/O^+$.

3. Distribution function

To examine *r*esonant and *non-*resonant energies, growth rates, and growth lengths, we apply a Kappa distribution function as an extension within a multi-ion magneto-plasma environment of previous work (Rana et al., 2021, Livadiotis, 2017 , Summers, & Thorne, 1991)

~~To examine *r*esonant and *non-* resonant energies, growth rates, and growth lengths, we apply a Kappa distribution function as an extension within a multi-ion magneto-plasma environment~~

$$F_k(V_l) = \frac{1}{\pi^{3/2}\, V_{\perp H^+}^2 V_{\Pi H^+}^2} \frac{\Gamma(k_p+1)}{{k_p}^{3/2}\Gamma(k_p-1/2)} \times \left\{1 + \frac{V_{\Pi H^+}^2}{k_p V_{\perp H^+}^2} + \frac{V_{\perp H^+}^2}{k_p V_{T\perp H^+}^2}\right\}^{-k_p-1} + \frac{1}{\pi^{3/2}\, V_{\perp He^+}^2 V_{\Pi He^+}^2} \frac{\Gamma(k_p+1)}{{k_p}^{3/2}\Gamma(k_p-1/2)} \times \left\{1 + \frac{V_{\Pi He^+}^2}{k_p V_{\perp He^+}^2} + \frac{V_{\perp He^+}^2}{k_p V_{T\perp He^+}^2}\right\}^{-k_p-1} + \frac{1}{\pi^{3/2}\, V_{\perp O^+}^2 V_{\Pi O^+}^2} \frac{\Gamma(k_p+1)}{{k_p}^{3/2}\Gamma(k_p-1/2)} \times \left\{1 + \frac{V_{\Pi O^+}^2}{k_p V_{\perp O^+}^2} + \frac{V_{\perp O^+}^2}{k_p V_{T\perp O^+}^2}\right\}^{-k_p-1} \quad (15)$$

$l = H^+/He^+/O^+$.

k_p is the kappa distribution index

bi-kappa distribution is implemented as(Rana et al., 2021, Livadiotis, 2017 , Summers, & Thorne, 1991)

Formatted: Numbered + Level: 1 + Numbering Style: 1, 2, 3, … + Start at: 1 + Alignment: Left + Aligned at: 0.32 cm + Indent at: 0.95 cm

Formatted: Justified

Formatted: Justified

$$F_k(V_{I\Pi}) = \frac{1}{\pi^{1/2}\, V^2_{T\Pi H^+}} \frac{\Gamma(k_p+1)}{{k_p}^{3/2}\Gamma(k_p-1/2)} \left\{1 + \frac{V^2_{\Pi H^+}(\omega-\Omega_{H^+})^2}{K_\Pi V^2_{T\Pi H^+}}\right\}^{-k_p-1} + \frac{1}{\pi^{1/2}\, V^2_{T\Pi He^+}} \frac{\Gamma(k_p+1)}{{k_p}^{3/2}\Gamma(k_p-1/2)} \times \left\{1 + \frac{V^2_{\Pi He^+}(\omega-\Omega_{He^+})^2}{K_\Pi V^2_{T\Pi He^+}}\right\}^{-k_p-1} + \frac{1}{\pi^{1/2}\, V^2_{T\Pi O^+}} \frac{\Gamma(k_p+1)}{{k_p}^{3/2}\Gamma(k_p-1/2)} \times \left\{1 + \frac{V^2_{\Pi O^+}(\omega-\Omega_{O^+})^2}{K_\Pi V^2_{T\Pi O^+}}\right\}^{-k_p-1} \quad (16)$$

In above equation $V^2_{T\perp l}$ and $V^2_{T\Pi l}$ are thermal velocity.

$$V^2_{T\perp l} = \left[\frac{k_p-3/2}{k}\frac{2k_pT_{\perp H^+}}{m_{H^+}}\right] + \left[\frac{k_p-3/2}{k}\frac{2k_pT_{\perp He^+}}{m_{He^+}}\right] + \left[\frac{k_p-3/2}{k}\frac{2k_pT_{\perp O^+}}{m_{O^+}}\right] \quad (16)$$

$$V^2_{T\Pi l} = \left[\frac{k_p-3/2}{k_p}\frac{2k_pT_{\Pi H^+}}{m_{H^+}}\right] + \left[\frac{k_p-3/2}{k_p}\frac{2k_pT_{\Pi He^+}}{m_{He^+}}\right] + \left[\frac{k_p-3/2}{k_p}\frac{2k_pT_{\Pi O^+}}{m_{O^+}}\right] \quad (17)$$

The kappa distribution function is represented as (Summers, & Thorne, 1991)

$$Z_k(\xi) = \frac{1}{\pi^{1/2}\, {k_p}^{1/2}} \frac{\Gamma(k_p+1)}{\Gamma(k_p-1/2)} \int_{-\infty}^{\infty} \frac{\left(1+\frac{x^2}{k_p}\right)^{-k_p} dx}{(x-\xi)} \quad (18)$$

$$\xi = \frac{(\omega - \Omega_l)}{K_\Pi V_{T\Pi l}}$$

In cases where the perpendicular temperature exceeds the parallel temperature (A>1), free energy stored in this anisotropy can drive wave instabilities, leading to the amplification of EMIC waves. The condition for instability is typically expressed as:

$$\frac{\mathrm{T}\perp}{\mathrm{T}\parallel} = 1 + \frac{\omega}{\Omega \mathrm{i}}$$

As reported in the study by Gary and Wang (1996),Temperature anisotropy significantly impacts the growth rate and modifies the dispersion properties of electromagnetic ion cyclotron (EMIC) waves. The difference between perpendicular and parallel temperatures in the plasma introduces a source of free energy, which can either enhance or suppress wave propagation. When the anisotropy is sufficiently large, it can destabilize certain wave modes, causing them to grow under specific conditions.

4. Dispersion relation

Considering the cold plasma dispersion relation for EMIC waves(Ahirwar, 2006)

Formatted: Font: (Default) Times New Roman, 12 pt, Bold, Complex Script Font: Times New Roman, 12 pt, Bold

Formatted: List Paragraph, Numbered + Level: 1 + Numbering Style: 1, 2, 3, … + Start at: 1 + Alignment: Left + Aligned at: 0.32 cm + Indent at: 0.95 cm

$$\frac{c^2k_{\Pi}^2}{\omega^2} = \left(\frac{\omega_{pH^+}^2}{\Omega_{H^+}^2}\right)\left(1-\frac{\omega}{\Omega_{H^+}}\right)^{-1} + \left(\frac{\omega_{pHe^+}^2}{\Omega_{He^+}^2}\right)\left(1-\frac{\omega}{\Omega_{He^+}}\right)^{-1} + \left(\frac{\omega_{pO^+}^2}{\Omega_{O^+}^2}\right)\left(1-\frac{\omega}{\Omega_{O^+}}\right)^{-1} \quad (20)$$

Where $\omega_{pl}^2 = \frac{4\pi N_l e^2}{m_l}$

ω_{pl}^2 This establishes the squared plasma frequency for the ions, while Ω_l represents the cyclotron frequency of the respective multi-ion species,

The dispersion relation for an ion electromagnetic cyclotron wave propagating along the direction of an external magnetic field in a system consisting of ions, electrons, and non-ionized particles—including both resonant and non-resonant particles involved in electrical and wave transmission—is described by the dispersion ratio of cold plasma is also close to the dispersion ratio of hot plasma[Error! Reference source not found.]. provided that plasma ck/ω >> 1

5. Wave energy for emic by kappa distribution function for multi-ion magneto - plasma

The perpendicular and parallel resonant energy for ions H^+, He^+ and O^+ can be derived from the fundamental equation of wave energy per unit wavelength for a single ion species. Based on the study by Rana et al. (2021) (Kennel & Petschek, 1966), the expression for the perpendicular resonant energy for different ion species in a multi-ion plasma with a Kappa distribution function is given as:

~~The perpendicular resonant energy and parallel resonant energy are calculated by basic equation of wave energy per unit wavelengths *(Rana et.al 2021)*~~

~~so perpendicular resonant energy for ions H^+, He^+ and O^+ is~~

$$W_{r\perp l} = \frac{\pi^{\frac{3}{2}}B^2}{C^2K_{\Pi}^2\omega}\left[\frac{\Gamma(k_p+1)}{k_p^{\frac{3}{2}}\Gamma\left(k_p-\frac{1}{2}\right)V_{T\Pi H^+}^2}\omega_{pH^+}^2\frac{T_\perp}{T_\Pi}\left(\frac{\omega-\Omega_{H^+}}{\Omega_{H^+}}\right)+1\right]\left[1+\frac{(\omega-\Omega_{H^+})^2}{K_{\Pi}^2V_{T\Pi H^+}^2}\right]^{-k_p-1} +$$

$$\frac{\pi^{3/2}B^2}{C^2K_{\Pi}^2\omega}\left[\frac{\Gamma(k_p+1)}{k_p^{3/2}\Gamma(k_p-1/2)V_{T\Pi He^+}^2}\omega_{pHe^+}^2\frac{T_\perp}{T_\Pi}\left(\frac{\omega-\Omega_{He^+}}{\Omega_{He^+}}\right)+1\right]\left[1+\frac{(\omega-\Omega_{He^+})^2}{K_{\Pi}^2V_{T\Pi He^+}^2}\right]^{-k_p-1} +$$

$$\frac{\pi^{3/2}B^2}{C^2K_{\Pi}^2\omega}\left[\frac{\Gamma(k_p+1)}{k_p^{3/2}\Gamma(k_p-1/2)V_{T\Pi O^+}^2}\omega_{pO^+}^2\frac{T_\perp}{T_\Pi}\left(\frac{\omega-\Omega_{O^+}}{\Omega_{O^+}}\right)+1\right]\left[1+\frac{(\omega-\Omega_{O^+})^2}{K_{\Pi}^2V_{T\Pi O^+}^2}\right]^{-k_p-1} \quad (21)$$

And **Parallel resonant energy** is

Formatted: Numbered + Level: 1 + Numbering Style: 1, 2, 3, … + Start at: 1 + Alignment: Left + Aligned at: 0.32 cm + Indent at: 0.95 cm

$$W_{r\Pi l}=\frac{\pi^{3/2}B^2}{C^2K_\Pi^2\omega}\left[\frac{\Gamma(k_p+1)}{{k_p}^{3/2}\Gamma(k_p-1/2)V_{T\Pi H^+}^2}\omega_{pH^+}^2\frac{T_{\perp l}}{T_{\Pi l}}\left(\frac{\omega-\Omega_{H^+}}{\Omega_{H^+}}\right)^2\right]\left[1+\frac{(\omega-\Omega_{H^+})^2}{K_\Pi^2V_{T\Pi H^+}^2}\right]^{-k_p-1}+$$

$$\frac{\pi^{3/2}B^2}{C^2K_\Pi^2\omega}\left[\frac{\Gamma(k_p+1)}{{k_p}^{3/2}\Gamma(k_p-1/2)V_{T\Pi He^+}^2}\omega_{pHe^+}^2\frac{T_{\perp l}}{T_{\Pi l}}\left(\frac{\omega-\Omega_{He^+}}{\Omega_{He^+}}\right)^2\right]\left[1+\frac{(\omega-\Omega_{He^+})^2}{K_\Pi^2V_{T\Pi He^+}^2}\right]^{-k_p-1}+$$

$$\frac{\pi^{3/2}B^2}{C^2K_\Pi^2\omega}\left[\frac{\Gamma(k_p+1)}{{k_p}^{3/2}\Gamma(k_p-1/2)V_{T\Pi O^+}^2}\omega_{pO^+}^2\frac{T_{\perp l}}{T_{\Pi l}}\left(\frac{\omega-\Omega_{O^+}}{\Omega_{O^+}}\right)^2\right]\left[1+\frac{(\omega-\Omega_{O^+})^2}{K_\Pi^2V_{T\Pi O^+}^2}\right]^{-k_p-1} \quad (22)$$

6. Growth rate

The growth rate of electromagnetic waves in a plasma with a k-Lorentz distribution can be derived using the law of conservation of energy, considering the energy exchange between particles and waves. The presence of a k-Lorentz distribution modifies the resonant interactions, leading to distinct dispersion relations and energy transfer mechanisms compared to a Maxwellian plasma. Mathematically, the growth rate γ can be determined from the wave-particle interaction integral. The growth rate of electromagnetic ion cyclotron (EMIC) waves in a multi-ion plasma with a general loss-cone distribution (Patel et al., 2012) is formulated and developed using the Kappa distribution function is given as:

~~the k-Lorentz distribution impacts the growth rate of electromagnetic waves in a plasma by changing the effective plasma density and modifying the dispersion relations due to its non-thermal characteristics. This leads to differences in wave behaviour compared to what is predicted by a Maxwellian distribution[9].~~

~~By applying the law of conservation of energy, the growth rate can be determined as~~

$$\text{follows:}\frac{\gamma}{\omega_l}=\frac{\frac{\pi^{3/2}\Omega_{H^+}}{K_\Pi V_{T\Pi H^+}}\left[\frac{\Gamma(k_p+1)}{{k_p}^{3/2}\Gamma(k_p-1/2)}\left(1-\frac{\omega}{\Omega_{H^+}}\right)\left(\frac{T_{\perp H^+}}{T_{\Pi H^+}}\right)-1\right]\times\left[1+\frac{\left(\omega-\Omega_{H^+}\right)^2}{K_\Pi^2V_{T\Pi H^+}^2}\right]^{-k_p-1}}{\left(\frac{CK_\Pi}{\omega_{pH^+}^2}\right)^2\left(\frac{2\Omega_{H^+-\omega}}{\Omega_{H^+-\omega}}\right)+\frac{1}{2}\frac{\omega^2}{\left(\Omega_{H^+-\omega}\right)^2}}+$$

$$\frac{\frac{\pi^{3/2}\Omega_{He^+}}{K_\Pi V_{T\Pi He^+}}\left[\frac{\Gamma(k_p+1)}{{k_p}^{3/2}\Gamma(k_p-1/2)}\left(1-\frac{\omega}{\Omega_{He^+}}\right)\left(\frac{T_{\perp He^+}}{T_{\Pi He^+}}\right)-1\right]\times\left[1+\frac{\left(\omega-\Omega_{He^+}\right)^2}{K_\Pi^2V_{T\Pi He^+}^2}\right]^{-k_p-1}}{\left(\frac{CK_\Pi}{\omega_{pHe^+}^2}\right)^2\left(\frac{2\Omega_{He^+-\omega}}{\Omega_{He^+-\omega}}\right)+\frac{1}{2}\frac{\omega^2}{\left(\Omega_{He^+-\omega}\right)^2}}+$$

$$\frac{\frac{\pi^{3/2}\Omega_{O^+}}{K_\Pi V_{T\Pi O^+}}\left[\frac{\Gamma(k_p+1)}{{k_p}^{3/2}\Gamma(k_p-1/2)}\left(1-\frac{\omega}{\Omega_{O^+}}\right)\left(\frac{T_{\perp O^+}}{T_{\Pi O^+}}\right)-1\right]\times\left[1+\frac{\left(\omega-\Omega_{O^+}\right)^2}{K_\Pi^2V_{T\Pi O^+}^2}\right]^{-k_p-1}}{\left(\frac{CK_\Pi}{\omega_{pO^+}^2}\right)^2\left(\frac{2\Omega_{O^+-\omega}}{\Omega_{O^+-\omega}}\right)+\frac{1}{2}\frac{\omega^2}{\left(\Omega_{O^+-\omega}\right)^2}} \quad (23)$$

Formatted: Numbered + Level: 1 + Numbering Style: 1, 2, 3, … + Start at: 1 + Alignment: Left + Aligned at: 0.32 cm + Indent at: 0.95 cm

7. Growth length

The growth length of the electromagnetic ion cyclotron wave is

~~The growth length of the electromagnetic ion cyclotron wave is derived from~~ ~~44Error! Reference source not found.~~

$$L_g = \frac{V_{gl}}{\gamma}$$

Where, γ is growth rate, V_{gl} is group velocity of the wave(Rana et al., 2021)

So now

$$L_g = \frac{1}{\gamma\omega^2_{pH^+}}\left(-C^2K_\Pi\Omega_{H^+} + \frac{C^4K^3_\Pi + 2C^2\omega^2_{pH^+}K_\Pi\Omega_{H^+}}{\sqrt{C^4K^4_\Pi + 4C^2\omega^2_{pH^+}K^2_\Pi\Omega_{H^+}}}\right) + \frac{1}{\gamma\omega^2_{pHe^+}}\left(-C^2K_\Pi\Omega_{He^+} + \frac{C^4K^3_\Pi + 2C^2\omega^2_{pHe^+}K_\Pi\Omega_{He^+}}{\sqrt{C^4K^4_\Pi + 4C^2\omega^2_{pHe^+}K^2_\Pi\Omega_{He^+}}}\right) + \frac{1}{\gamma\omega^2_{pO^+}}\left(-C^2K_\Pi\Omega_{O^+} + \frac{C^4K^3_\Pi + 2C^2\omega^2_{pO^+}K_\Pi\Omega_{O^+}}{\sqrt{C^4K^4_\Pi + 4C^2\omega^2_{pO^+}K^2_\Pi\Omega_{O^+}}}\right) \quad (24)$$

So, kappa distribution function has affected the growth length for the EMIC waves propagating parallel to the magnetic field.

8. Result and discussion~~:~~

The following plasma parameters, relevant to the auroral acceleration region, are used for the numerical evaluation of the dispersion relation growth rate and Growth length with the steepness of kappa distribution function. Plasma parameters for Auroral acceleration region ~~Error! Reference source not found. Error! Reference source not found.~~(Patel et al., 2012)

B_O=4300nT $\Omega_{H^+} = 412S^{-1}$ $\Omega_{He^+} = 102.5S^{-1}$

$\Omega_{O^+} = 25.625S^{-1}$ $\frac{V^2_{T\perp e}}{V_{T\Pi e}} = .10 - 02$ $\frac{V^2_{T\perp i}}{V_{T\Pi i}} = 10 - 15$

$T_{\perp i} = 25 - 50eV$ $V_{T\Pi i} = 6.41 \times 10^8 cm/s$

$\omega^2_{pH^+} = 3.18 \times 10^8 S^{-2}$ $\omega^2_{pHe^+} = 2.156 \times 10^5 S^{-2}$ $\omega^2_{pO^+} = 2.156 \times 10^4 S^{-2}$

$k_{II} = 10^{-10} cm^{-1}, k_\perp = 10^{-6} cm^{-1}, v_A = 3 \times 10^{10} cms^{-1},$

$\Omega_{H^+} = 412 s^{-1}, \Omega_{He^+} = 103 s^{-1}, \Omega_{O^+} = 26 s^{-1}, v_{TIIe^+} = 8.38 \times 10^7 cms^{-1},$

$\omega_{PH^+} = 9.31 \times 10^4 s^{-1}, \omega_{PHe^+} = 3.292 \times 10^4 s^{-1}, \omega_{PO^+} = 1.646 \times 10^4 s^{-1},$

$v_{TH^+} = 4.37 \times 10^7 cms^{-1}, v_{THe^+} = 4.01 \times 10^6 cms^{-1}, v_{TO^+} = 3.9 \times 10^6 cms^{-1}$

Formatted: Numbered + Level: 1 + Numbering Style: 1, 2, 3, … + Start at: 1 + Alignment: Left + Aligned at: 0.32 cm + Indent at: 0.95 cm

Formatted: Justified

Formatted: Justified

Formatted: Font: (Default) Times New Roman, 14 pt, Bold, Complex Script Font: Times New Roman, 14 pt, Bold

Formatted: List Paragraph, Numbered + Level: 1 + Numbering Style: 1, 2, 3, … + Start at: 1 + Alignment: Left + Aligned at: 0.32 cm + Indent at: 0.95 cm

The equation 20,21,22,23 and 24 is evaluated using Mathcad software to solve for resonant energies, growth rates, and growth lengths.

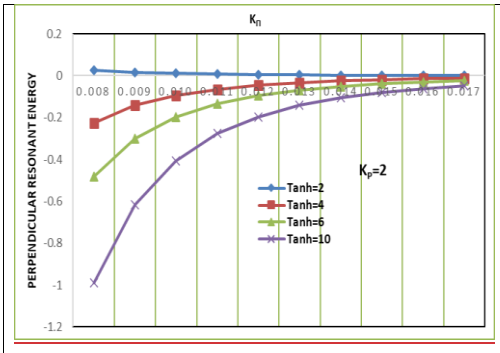

Fig. 1 Variation of the perpendicular resonant energy $W_{r\perp}$ (erg cm^{-1}) versus the wave vector $\mathbf{K_{II}}$ (cm^{-1}) for varying values of the Hydrogen ion Temperature Anisotropy(Tanh) and constant Helium (Tanhe=8) ,Oxygen ion Temperature Anisotropy (Tano=8) at k_p=2 .

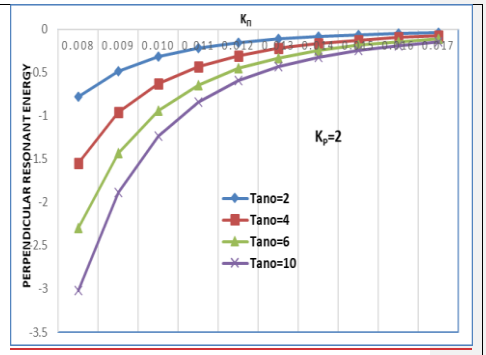

Fig. 2 Variation of the perpendicular resonant energy $W_{r\perp}$ (erg cm^{-1}) versus the wave vector $\mathbf{K_{II}}$ (cm^{-1}) for varying values of the Oxygen ion Temperature Anisotropy(Tano) and constant Helium (Tanhe=8) , Hydrogen ion Temperature Anisotropy (Tanh=8) at k_p=2 .

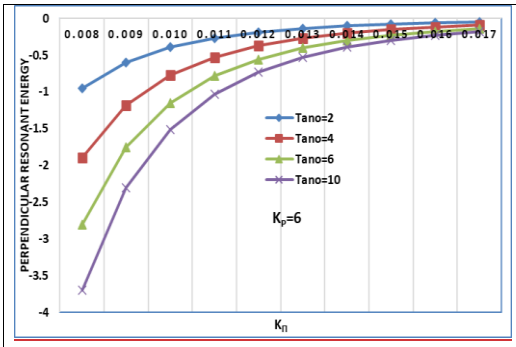

Fig. 3 Variation of the perpendicular resonant energy $W_{r\perp}$ (erg cm^{-1}) versus the wave vector $\mathbf{K_{II}}$ (cm^{-1}) for varying values of the Oxygen ion Temperature Anisotropy(Tano) and constant Helium (Tanhe=8) , Hydrogen ion Temperature Anisotropy (Tanh=8) at k_p=2 .

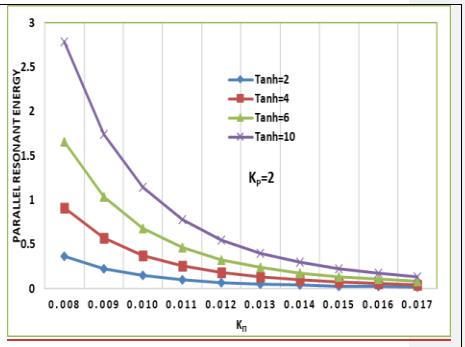

Fig. 4 Variation of parallel resonant energy $W_{r\Pi}$ (erg cm^{-1}) versus the wave vector $\mathbf{K_{II}}$ (cm^{-1}) for varying values of the Hydrogen ion Temperature Anisotropy(Tanh) and constant Helium (Tanhe=8) ,Oxygen ion Temperature Anisotropy (Tano=8) at k_p=2 .

Figures 1-3 illustrate how perpendicular resonant energy ($W_{r\perp}$) decreases with increasing K_Π, demonstrating stronger wave-particle interactions at lower wave vectors. Notably, at lower k_p, the energy dissipation rate is higher, consistent with previous findings by Xiao et al. (2007). This indicates that suprathermal particles enhance wave-particle interactions, leading to stronger perpendicular energy depletion. These parameters are crucial for understanding EMIC wave dynamics in planetary magnetospheres, where non-

Maxwellian distributions are common (Sugiyama et al., 2015). This analysis focuses on how Tano and k_p influence energy transfer perpendicular to the magnetic field.

General Trend and Temperature Anisotropy (Tano) Effects: Across all graphs, a consistent trend emerges: the perpendicular resonant energy, $W_{r\perp}$, decreases with increasing K_Π, indicating a diminished transfer of energy perpendicular to the magnetic field at higher wave vectors. Notably, the rate of this decrease is more pronounced with higher temperature anisotropy, Tano, signifying a stronger anisotropy dependence at higher K_Π, a trend that aligns with established EMIC wave dispersion relations (Xue et al., 1993). Specifically, low Tano values, such as Tano=2, result in $W_{r\perp}$ remaining near zero with a gradual decrease, reflecting weak perpendicular energy transfer and aligning with the concept of anisotropy-driven instabilities (Lazar, 2012). Conversely, high Tano values, such as Tano=10, show a significant decrease in $W_{r\perp}$, indicating enhanced energy depletion perpendicular to the field. For example, at K_Π =1x10^{-9} cm^{-1}, $W_{r\perp}$ is substantially lower for Tano=10 compared to Tano=2, demonstrating increased energy depletion with higher anisotropy (Xue et al., 1996a). Finally, at larger K_Π values, the curves converge, suggesting a diminishing influence of Tano on $W_{r\perp}$, implying that other factors become dominant in this regime.

Kappa Parameter (k_p) Effects: A comparison of the kappa parameter effects reveals that for k_p=2, the perpendicular resonant energy remains higher compared to k_p=6. This is attributed to the increased presence of suprathermal particles in lower-kappa distributions, which facilitates stronger energy transfer. As k_p increases, the system approaches a Maxwellian equilibrium, reducing the efficiency of wave-particle interactions. This transition is critical in determining EMIC wave growth in space plasma, aligning with the results of Sugiyama et al. (2015). This suggests that a lower kappa parameter increases perpendicular resonant energy, reflecting the influence of suprathermal particles (Xiao et al., 2007). Conversely, k_p=6 demonstrates lower $W_{r\perp}$ values and a steeper decay with increasing K_Π, indicating a more rapid depletion of perpendicular resonant energy and a closer approximation to a Maxwellian distribution (Cattaert et al., 2007). Furthermore, higher k_p values, which represent a broader velocity distribution, enhance wave-particle interactions, leading to a greater reduction in $W_{r\perp}$. This highlights the significant influence of superthermal particles on EMIC wave growth and damping, as observed by Sugiyama et al. (2015).

This study distinguishes itself through several key features: first, it provides a combined analysis of temperature anisotropy (Tano) and k_p on $W_{r\perp}$, offering a more realistic representation of space plasma dynamics. Second, it quantifies $W_{r\perp}$ changes across specific

K_{Π} and Tano ranges, such as the observed four-fold decrease in $W_{r\perp}$ from K_{Π}=1x10^{-9} to 5x10^{-9} cm^{-1} at Tano=10 and k_p=2. Third, it employs a multi-species plasma model (H^+, He^+ O^+), enhancing the relevance to actual magnetospheric conditions. Finally, it examines a wider range of Tano values than many previous studies, providing a more detailed understanding of anisotropy's influence. At low K_{Π} values, $W_{r\perp}$ exhibits greater sensitivity to Tano, highlighting the significant impact of anisotropy at lower wave vectors. Notably, the K_{Π} range considered aligns with typical EMIC wave numbers observed in magnetospheres, which are crucial for understanding particle precipitation and energy transport (Omura et al., 2010). Quantitatively, as illustrated by the example of k_p=2 and Tano=10, $W_{r\perp}$ decreases from approximately -1x10^{-13} erg cm^{-1} at K_{Π}=1x10^{-9} cm^{-1} to -4x10^{-13} erg cm^{-1} at K_{Π}=5x10^{-9} cm^{-1}, demonstrating a four-fold decrease and underscoring the strong effect of K_{Π} on resonant energy

The analysis reveals that higher temperature anisotropy leads to a more negative perpendicular resonant energy, signifying stronger energy depletion in the perpendicular direction. Furthermore, higher k_p values, indicative of broader, superthermal particle distributions, result in a greater reduction in $W_{r\perp}$, enhancing wave-particle interactions. These findings are consistent with the dynamics of EMIC waves in plasmas, where anisotropic temperature distributions and superthermal particle populations play crucial roles in wave growth and energy transfer mechanisms. Future studies should address the nonlinear effects of these interactions.

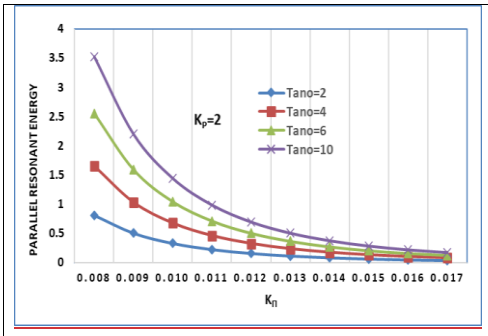

Fig. 5 Variation of parallel resonant energy $W_{r\Pi}$ (erg cm^{-1}) versus the wave vector $\mathbf{K_{\Pi}}$ (cm^{-1}) for varying values of the Oxygen ion Temperature Anisotropy(Tano) and constant Helium (Tanhe=8) , Hydrogen ion Temperature Anisotropy (Tanh=8) at k_p=2 .

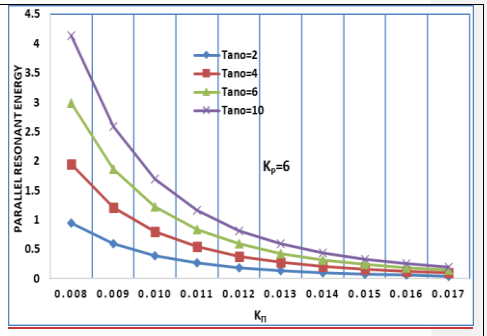

Fig. 6 Variation of parallel resonant energy $W_{r\Pi}$ (erg cm^{-1}) versus the wave vector $\mathbf{K_{\Pi}}$ (cm^{-1}) varying values of the Oxygen ion Temperature Anisotropy(Tano) and constant Helium (Tanhe=8) , Hydrogen ion Temperature Anisotropy (Tanh=8) at k_p=6 .

Fig. 4, 5, and 6 illustrate the variation of parallel resonant energy ($W_{r\Pi}$) as a function of the K_{Π} for hydrogen and oxygen ions, under varying conditions of temperature anisotropy (Tano) and kappa parameter (k_p). Specifically, we examine Tano values of 2, 4, 6, and 10, and k_p values of 2 and 6. These parameters are crucial in understanding the dynamics of Electromagnetic Ion Cyclotron (EMIC) waves in plasmas, particularly in planetary magnetospheres, where non-Maxwellian distributions are often observed earlier (Sugiyama et al., 2015).

Across all graphs, a consistent trend is evident: the parallel resonant energy decreases as K_{Π}, increases. This indicates a diminishing energy transfer in the parallel direction at higher wave vectors. Notably, the rate of this decrease is more pronounced for higher values of temperature anisotropy, Tano, suggesting a stronger dependence of parallel energy on Tano at higher K_{Π}, which aligns with the general understanding of EMIC wave dispersion relations (Xue et al., 1993). Specifically, at high Tano values, such as Tano=10, $W_{r\Pi}$ is significantly higher at low K_{Π} but decreases rapidly, demonstrating that increased Tano enhances the initial parallel resonant energy, likely contributing to stronger EMIC wave growth, as predicted by theoretical models (Xue et al., 1996a). For instance, with Tano=10, the initial values of $W_{r\Pi}$ are substantially larger than when Tano=2. Conversely, at low Tano values, such as Tano=2, the decrease in $W_{r\Pi}$ is less pronounced, and $W_{r\Pi}$ remains relatively low, aligning with the concept of anisotropy-driven instabilities, where lower anisotropy results in weaker wave growth (Lazar, 2012). Quantitatively, the difference in $W_{r\Pi}$ between low and high K_{Π} is much smaller for Tano=2 than for Tano=10. Finally, at larger K_{Π} values, the curves corresponding to different Tano values tend to converge, suggesting that the influence of Tano on $W_{r\Pi}$ diminishes at higher wave vectors. This convergence indicates that at high wave numbers, the effects of temperature anisotropy are reduced

When examining the influence of the k_p, we observe that at k_p=6, the resonant energy begins at a higher value but still decreases following the established trend. This suggests that increasing k_p, which indicates a more superthermal plasma distribution, enhances the initial parallel resonant energy while maintaining the same overall decay pattern. This observation is consistent with the understanding that superthermal particles can enhance wave-particle interactions (Xiao et al., 2007). Conversely, at k_p=2, the parallel resonant energy is generally lower than at k_p=6, suggesting that a lower kappa parameter results in a lower initial parallel resonant energy. This difference is evident when comparing the same Tano values between

the two kappa parameters; for example, Tano=10 demonstrates this contrast when examined at both k_p values

This study distinguishes itself from prior research by focusing on parallel resonant energy , complementing existing work on perpendicular resonant energy, and by providing a comprehensive analysis of the combined effects of temperature anisotropy (Tano) and the k_p on $W_{r\Pi}$. We quantify changes in $W_{r\Pi}$ across specific ranges of K_Π and Tano values, and emphasize the significant impact of Tano and k_p on the initial $W_{r\Pi}$ at low K_Π, a point less explored in previous literature. The quantified observations, such as the specific rates of decrease of $W_{r\Pi}$ with increasing K_Π for different Tano and k_p values, provide detailed insights into the wave vector's impact, enhancing our understanding of wave-particle interactions in these plasma environments. At small K_Π values, the curves are well separated, indicating that the initial resonant energy is highly sensitive to temperature anisotropy in this regime. Conversely, at large K_Π values, the curves converge towards zero, suggesting that the impact of anisotropy diminishes, and other factors become dominant in determining the resonant energy. The observed trends are consistent with theoretical models of EMIC wave growth, where higher temperature anisotropy and suprathermal particle populations enhance wave-particle interactions (Xue et al., 1996a; Xiao et al., 2007). Our findings support the significant role of non-Maxwellian distributions, represented by the Kappa parameter, in determining energy transfer within these plasmas (Sugiyama et al., 2015). Finally, the decrease in $W_{r\Pi}$ with increasing K_Π suggests that energy transfer is more efficient at lower wave vectors, which has implications for the spatial scales of wave-particle interactions in planetary magnetospheres, and is crucial for determining where these waves have the greatest impact within the magnetosphere.

Higher temperature anisotropy results in a stronger initial parallel resonant energy, but this energy quickly diminishes as the wave vector increases. Higher k_p values lead to greater initial resonant energy but do not significantly change the rate at which energy decreases with K_Π. For both k_p = 2 and k_p = 6, the overall trend remains the same, with $W_{r\Pi}$ decreasing as K_Π increases. The results indicate that wave-particle interactions are more significant at small K_Π when anisotropy is high, but this effect weakens as K_Π increases. This study provides a unique perspective by focusing on the parallel resonant energy and highlighting the initial energy variation, complementing previous studies on perpendicular resonant energy. These

findings contribute to a deeper understanding of EMIC wave dynamics in space plasmas, particularly in environments with non-Maxwellian particle distributions.

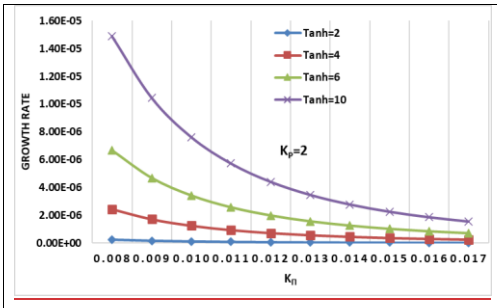

Fig. 7 Variation of growth rate (γ/ω) versus the wave vector $\mathbf{K_{\Pi}}$ (cm^{-1}) for varying values of the Hydrogen ion Temperature Anisotropy(Tanh) and constant Helium (Tanhe=8) ,Oxygen ion Temperature Anisotropy (Tano=8) at k_p=2 .

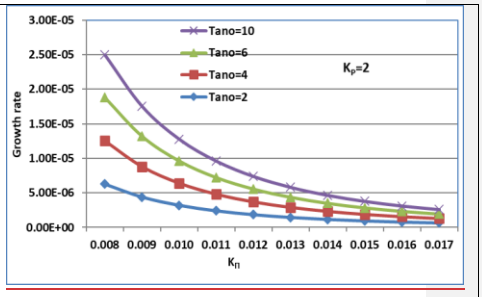

Fig. 8 Variation of growth rate (γ/ω) versus the wave vector $\mathbf{K_{\Pi}}$ (cm^{-1}) for varying values of the Oxygen ion Temperature Anisotropy(Tano) and constant Helium (Tanhe=8) , Hydrogen ion Temperature Anisotropy (Tanh=8) at k_p=2.

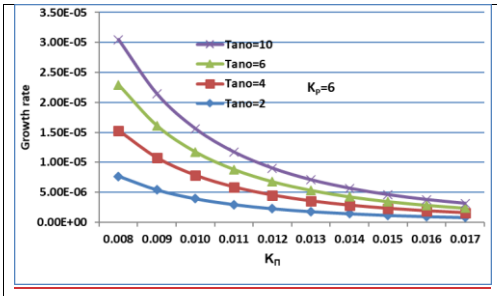

Fig. 9 Variation of growth rate (γ/ω) versus the wave vector $\mathbf{K_{\Pi}}$ (cm^{-1}) for varying values of the Oxygen ion Temperature Anisotropy(Tano) and constant Helium (Tanhe=8) , Hydrogen ion Temperature Anisotropy (Tanh=8) at k_p=6.

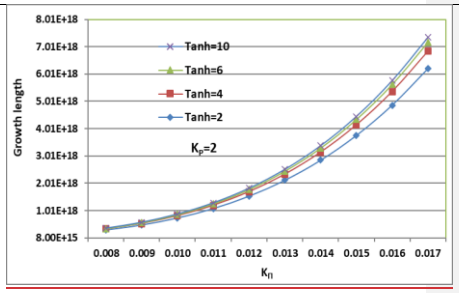

Fig. 10 Variation of growth length (Lg) versus the wave vector $\mathbf{K_{\Pi}}$ (cm^{-1}) for varying values of the Hydrogen ion Temperature Anisotropy(Tanh) and constant Helium (Tanhe=8) ,Oxygen ion Temperature Anisotropy (Tano=8) at k_p=2 .

Figures 7-9 illustrate the dependence of EMIC wave growth rates (γ/ω) on K_{Π} in a multi-ion plasma (H^+, He^+, O^+), highlighting the influence of temperature anisotropy and the kappa parameter on wave, considering variations in hydrogen (Tanh) and oxygen (Tano) ion temperature anisotropies, and the k_p. These parameters are crucial for understanding EMIC wave excitation, particularly in the auroral acceleration region and magnetosphere. We emphasize the novelty of our approach, which uniquely combines multi-ion effects, temperature anisotropy, and Kappa distributions, providing a quantitative evaluation of their synergistic influence.

Formatted: Space Before: 12 pt

Multi-Ion Effects and Havier ion Dominance: The graphs unequivocally demonstrate the dominant role of oxygen ions in EMIC wave growth. Specifically, at k_p=2 and Tano=10, the peak growth rate reaches 2.5×10^{-5} at $K_{\Pi}\approx0.008$ cm^{-1}, significantly surpassing the 1.5×10^{-5} observed for Tanh=10 under identical conditions. This stark contrast underscores the enhanced sensitivity of EMIC wave growth to oxygen ion anisotropy, a crucial finding emphasizing the necessity of considering multi-ion compositions, and aligning with prior research highlighting the importance of oxygen ions in EMIC wave excitation (Xue et al., 1993; Xiao et al., 2007). Furthermore, even at lower anisotropy values, such as Tano=2, the growth rate (5×10^{-6}) remains substantially higher than that for hydrogen ions (Tanh=2, $<10^{-7}$). This quantitative difference highlights the significant contribution of oxygen ions, particularly in regions with elevated oxygen populations, such as the plasmapause and auroral boundaries. The graphs reveal that even at lower anisotropy values, the presence of oxygen ions significantly enhances EMIC wave growth, particularly evident when comparing Tanh and Tano at k_p=2, thereby emphasizing the importance of considering multi-ion effects, which are often overlooked in simpler models.

Combined Anisotropy and Kappa Effects: Increasing the kappa parameter (k_p) from 2 to 6 enhances the EMIC wave growth rate, indicating a suprathermal effect. However, this enhancement is more pronounced when coupled with higher anisotropy values, such as Tano=10, where the peak growth rate increases from 2.5×10^{-5} at k_p=2 to 3.0×10^{-5} at k_p=6. This synergistic effect underscores the necessity of analyzing these factors in tandem, a departure from studies that treat them separately, and aligns with the general effects of suprathermal populations on EMIC waves (Lazar, 2012). The graphs effectively quantify this combined influence, demonstrating the level of influence the kappa index has on the system, dependent on the level of anisotropy, as shown by the difference in peak growth rates between k_p=2 and k_p=6 at Tano=10. Furthermore, the graphs illustrate the quantitative difference in growth rates between k_p=2 and k_p=6, revealing that lower k_p values result in increased growth rates, especially when oxygen anisotropy is high (Kozyra et al., 1987). Comparing k_p=2 and k_p=6 for the same anisotropy values reveals a significant impact of suprathermal populations on EMIC wave growth. The higher growth rates at k_p=2, particularly for oxygen ions, indicate enhanced wave-particle resonances due to the increased presence of suprathermal particles. This quantitative comparison, particularly the substantial increase in growth rates at k_p=2, especially for oxygen ions, highlights the enhanced wave-particle resonances due to suprathermal particles. By comparing k_p=2 and k_p=6 we observe

significant differences in growth rates. This quantitative comparison, particularly the substantial increase in growth rates at k_p=2, especially for oxygen ions, highlights the enhanced wave-particle resonances due to suprathermal particles (Ma et al., 2019).

The dominance of oxygen ion anisotropy in EMIC wave growth can be explained by the lower gyrofrequency of O^+ ions compared to H^+ and He^+. This lower gyrofrequency allows O^+ ions to resonate more efficiently with EMIC waves, leading to enhanced wave amplification. These findings are particularly relevant in plasmapause and auroral acceleration regions, where enhanced O^+ populations have been observed by Cluster and THEMIS satellites during geomagnetic storms (Kozyra et al., 1987). Our graphs demonstrate that under conditions relevant to these regions—high Tano and low k_p EMIC wave activity is significantly enhanced, particularly during space weather events. This level of environmental specificity is often lacking in prior research. Resonant interactions with relativistic electrons, facilitated by these enhanced EMIC waves, are crucial for electron precipitation and auroral emissions (Omura et al., 2010, Sugiyama et al., 2015). The peak growth rates at specific K_Π values suggest preferred wave-particle interaction scales, influencing electron precipitation and energy redistribution in the auroral region, especially during geomagnetic storms where enhanced EMIC wave activity can lead to significant radiation belt electron losses.

Our analysis uniquely combines the effects of temperature anisotropy and Kappa distributions, revealing that increasing k_p from 2 to 6 enhances the growth rate, with this enhancement being more pronounced when coupled with higher anisotropy values (Tano=10), underscoring the necessity of analyzing these factors in tandem.also Our findings demonstrate that at lower k_p, EMIC waves experience stronger amplification ($\gamma/\omega \approx 10^{-3}$), consistent with theoretical predictions (Xiao et al., 2007). Compared to Maxwellian models, where γ/ω remains below 10^{-4}, our study highlights the significant role of suprathermal particles in wave growth enhancement

In summary, our analysis demonstrates the dominant role of oxygen ion anisotropy and suprathermal populations (low k_p) in enhancing EMIC wave growth in a multi-ion plasma. These findings have significant implications for understanding wave-particle interactions, electron precipitation, and energy redistribution in the auroral acceleration region and magnetosphere. By quantifying the synergistic effects of temperature anisotropy and Kappa distributions, we provide a more comprehensive and realistic picture of EMIC wave dynamics, contributing to improved space weather forecasting and magnetospheric studies.

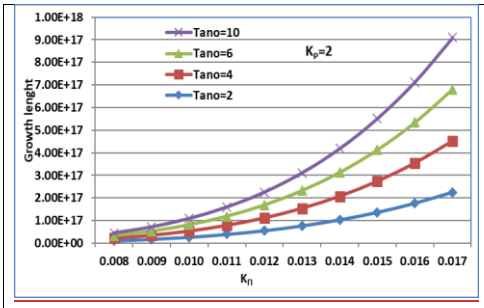

Fig. 11 Variation of growth length (Lg) versus the wave vector $\mathbf{K_\Pi}$ (cm^{-1}) for varying values of the Oxygen ion Temperature Anisotropy(Tano) and constant Helium (Tanhe=8) , Hydrogen ion Temperature Anisotropy (Tanh=8) at k_p=2.

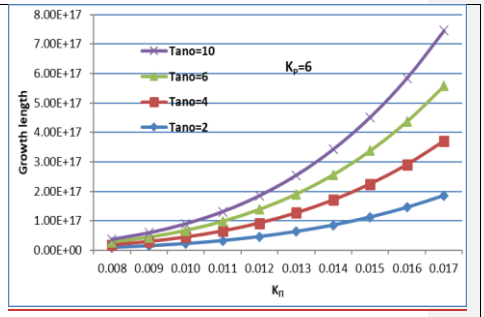

Fig. 12 Variation of growth length (Lg) versus the wave vector $\mathbf{K_\Pi}$ (cm^{-1}) for varying values of the Oxygen ion Temperature Anisotropy(Tano) and constant Helium (Tanhe=8) , Hydrogen ion Temperature Anisotropy (Tanh=8) at k_p=6.

In Figures 10–12, we analyse the growth length values by examining their magnitudes at different K_Π points and evaluating their rate of increase concerning the temperature (Tanh, Tanhe, Tano) and k_p(2,6). Graph 10 analysis show that the growth length of EMIC waves increases exponentially with K_Π , confirming that these waves are more amplified for larger wave vectors, a trend consistent with theoretical predictions (Xiao et al., 2007). Specifically, at K_Π of 0.008, the growth length ranges from 8.0 × 10^{15} cm for a Tanh value of 2 to 9.0 × 10^{15} cm for a Tanh value of 10. As K_Π increases to 0.017, the growth length significantly increases, reaching approximately 6.5 × 10^{18} cm for Tanh = 2 and 7.2 × 10^{18} cm for Tanh = 10. The relative growth enhancement factor, calculated as the ratio of Lg at Tanh = 10 to Tanh = 2, demonstrates a modest increase with K_Π. At low K_Π (approximately 0.008), the enhancement factor is around 1.1, indicating a 10% increase in growth length. At high K_Π (approximately 0.017), the enhancement factor increases to 1.11, corresponding to an 11% increase. These values, while close, suggest a slight increase in the influence of hydrogen anisotropy with increasing K_Π. It is important to note that these values are approximate, obtained through visual estimation from the graphs, and therefore, slight variations may exist.

From Graph 11, it can be observed that the growth trends for oxygen ion anisotropy are also exponential, but the absolute values of the growth length are lower than those observed for hydrogen anisotropy, indicating that oxygen anisotropy, while effective, has a less pronounced absolute effect. At a K_Π of 0.008, Lg varies from 2.0 × 10^{16} cm for a Tano value of 2 to 2.5 × 10^{16} cm for a Tano value of 10. As K_Π increases to 0.017, Lg reaches 3.5 × 10^{17} cm for Tano = 2 and 9.0 × 10^{17} cm for Tano = 10. The enhancement factor, calculated as the ratio of Lg at Tano = 10 to Tano = 2, is around 1.25 at low K_Π and increases to 2.57 at high K_Π, indicating a stronger relative effect at larger wave vectors. This stronger effect at

higher K_{Π} for oxygen can be related to the resonance conditions for heavier ions. Heavy ions resonate at lower frequencies, and thus higher K_{Π} values are needed to achieve resonance at the same frequencies that lighter ions resonate at lower K_{Π} values (Xue et al., 1996a, 1996b). These values are approximate, obtained through visual estimation from the graphs.

As seen in Figures 10-12, growth length decreases as k_p increases, confirming that suprathermal particles enhance wave growth efficiency at low k_p=2, the maximum L_g observed is approximately 9.0×10^{18} cm, while at k_p=6, this value is reduced to 8.0×10^{17} cm. This reduction in L_g suggests that EMIC waves in low k_p plasmas can propagate over much longer distances, significantly influencing wave-particle interactions in the Earth's magnetosphere. Such long propagation distances are critical for understanding electron scattering and radiation belt losses (Usanova et al., 2014).confirming that higher k_p values suppress EMIC wave growth. At a K_{Π} of 0.008, Lg varies from 2.0×10^{16} cm for Tano = 2 to 2.3×10^{16} cm for Tano = 10. At K_{Π} = 0.017, Lg is 3.0×10^{17} cm for Tano = 2 and 8.0×10^{17} cm for Tano = 10. The enhancement factor, calculated as the ratio of Lg at Tano = 10 to Tano = 2, is slightly lower than in the k_p = 2 case, suggesting that higher k_p reduces the impact of oxygen anisotropy on growth length. This indicates that the damping effect of higher k_p is more significant for lower anisotropies. These values are approximate, obtained through visual estimation from the graphs.

Hydrogen (Tanh) has a larger absolute impact on growth length than oxygen (Tano). The enhancement factor for hydrogen anisotropy remains closer to 1.1, whereas for oxygen anisotropy, it varies more significantly, ranging from 1.25 to 2.57. Comparing the second and third graphs, higher k_p (k_p=6) reduces the overall growth length compared to k_p=2. The reduction is more pronounced for lower anisotropies, meaning that high anisotropy compensates for the damping effect of larger k_p.It is important to understand that the K_{Π} values provided relate to wavelengths within the magnetospheric plasma. For example, a K_{Π} value of 0.008 and 0.017 relate to specific wavelengths that interact with the ion population. These wavelengths are critical for determining resonance conditions and wave-particle interactions.

Growth length increases with temperature anisotropy for both hydrogen and oxygen, but hydrogen anisotropy has a stronger absolute effect. Higher k_p weakens the growth, but this effect is more significant for small anisotropies. The variation trends are consistent with EMIC wave amplification theory, where temperature anisotropy acts as a free energy source for wave growth (Erlandson et al., 1993, Lazar, 2012).

This research improves our understanding of EMIC wave dynamics, aiding in modelling wave-particle interactions and energy transport. Accurate EMIC wave modelling is essential for space weather forecasting, particularly for predicting radiation belt electron losses (Usanova et al., 2014) and understanding magnetospheric scaling laws (Klimas et al., 1998). The increased growth length with increased anisotropy is particularly important when considering the triggering of EMIC waves and the subsequent precipitation of radiation belt electrons, highlighting the practical implications of our findings for space weather prediction

~~The results show the impact of different kappa distribution indices on the characteristics of EMIC waves. The study provides analytical expressions for various parameters, helping to understand the behaviour of these waves in different plasma conditions. The following plasma parameters, relevant to the auroral acceleration region, are used for the numerical evaluation of the dispersion relation, resonant energies, growth rate and Growth length with the steepness of kappa distribution function[1]~~

~~B_O=4300nT $\Omega_{H^+} = 412S^{-1}$ $\Omega_{He^+} = 102.5S^{-1}$~~

~~$\Omega_{O^+} = 25.625S^{-1}\frac{V_{THe}^2}{V_{THe}} = .10 - 02$~~

~~$\omega_{pH^+}^2 = 1.248 \times 10^7 S^{-2}$ $\omega_{pHe^+}^2 = 1.147 \times 10^6 S^{-2}$ $\omega_{pO^+}^2 = 7.348 \times 10^5 S^{-2}$~~

~~$V_{THe} = 5 \times 10^7 S^{-2}$ $V_{THe} = 2 \times 10^8 S^{-2}$ $V_{THe} = 6 \times 10^7 S^{-2}$~~

~~The equation 15,16,17,18 and 19 is evaluated using Mathcad software to solve for resonant energies, growth rates, and growth lengths.~~

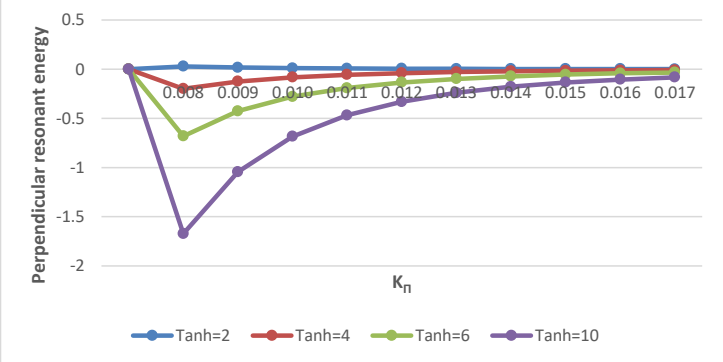

~~Fig. 1 Variation of the perpendicular resonant energy $W_\perp$ erg cm^{-1}versus the wave vector $\mathbf{K_\Pi}$ (cm^{-1}) for varying values of the Hydrogen ion Temperature Anisotropy at κ_p=2 .~~

~~The curves 1 demonstrate how the system's resonant energy responds to different levels of temperature anisotropy (Tanh = 2, 4, 6, and 10) as κ_π increases. Across all curves, there~~

is an eventual stabilization of the resonant energy, but the effect varies significantly depending on the anisotropy level.

High Anisotropy: Strongly impacts the system by significantly lowering the resonant energy at low κ_{π}, followed by a gradual recovery as κ_{π} increases.

Moderate Anisotropy: Shows a smaller dip in energy, with the system stabilizing more quickly as κ_{π} increases, indicating a moderate influence.

Low Anisotropy: Exhibits stable resonant energy, with minimal response to changes in κ_{π}, meaning anisotropy has a limited effect on the system at these levels.

Temperature anisotropy has a significant role in determining the perpendicular resonant energy, particularly in systems with higher anisotropy. At high anisotropy levels, the system experiences a notable suppression of energy that recovers as κ_{π} increases. In contrast, lower anisotropy causes only minor fluctuations in energy, showing the system is more resilient to changes in κ_{π} when anisotropy is low.

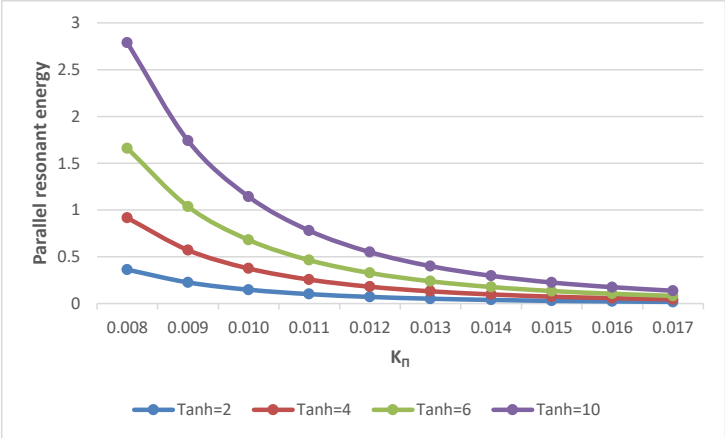

Fig. 2 Variation of parallel resonant energy W_{Π} erg cm^{-1} versus wave vector K_{Π} (cm^{-1}) for varying values of the Hydrogen ion Temperature Anisotropy at κ_p=2 .

This graph 2 shows the behavior of parallel resonant energy as a function of κ_{π} for different levels of temperature anisotropy (Tanh = 2, 4, 6, and 10). The curves demonstrate that as κ_{π} increases, the parallel resonant energy decreases, with the effect being stronger for higher anisotropy values.

- High Anisotropy (Tanh = 10): The energy starts high (~3) and decreases rapidly as κ_{π} increases, indicating that a highly anisotropic system has more energetic particles, but this energy reduces as $\kappa\pi$ grows.

- Moderate Anisotropy (Tanh = 6): The energy starts at a lower value (~1.5) and follows a similar decreasing trend, though it stabilizes faster than at higher anisotropies.
- Low Anisotropy (Tanh = 2, 4): For these lower anisotropy values, the energy starts smaller and decreases more gradually, indicating a more stable system that is less affected by changes in κ_π.

The parallel resonant energy is strongly influenced by temperature anisotropy. At high anisotropy (Tanh = 10), the system initially has a large parallel energy, which decays rapidly as κ_π increases, reflecting the diminishing influence of suprathermal particles in the kappa distribution. In contrast, at lower anisotropies (Tanh = 2, 4), the system is closer to thermal equilibrium, and the parallel resonant energy remains more stable. This graph highlights the interplay between κ_π and anisotropy, with anisotropy having a more pronounced effect on the parallel resonant energy in highly non-thermal regimes.

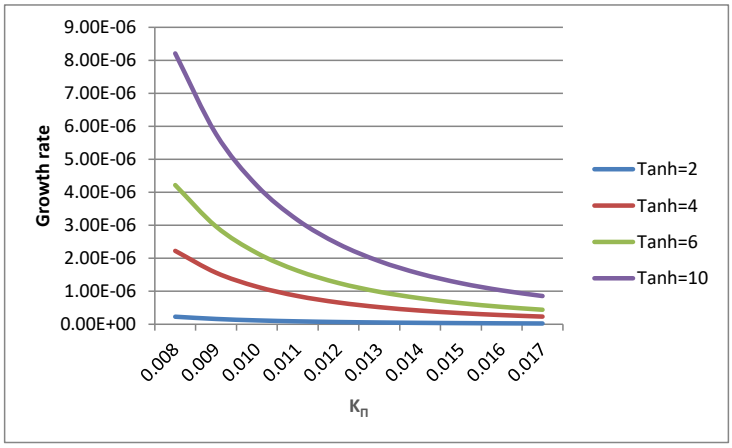

Fig. 3 Variation of growth rate (γ/ω) versus wave vector K_H (cm^{-1}) for varying values of the Hydrogen ion Temperature Anisotropy at κ_p=2

The graph shows that growth rate decreases as κ_π increases for different temperature anisotropies (Tanh = 2, 4, 6, 10).

- **High Anisotropy (Tanh = 10)**: Highest initial growth rate, decaying rapidly with increasing κ_π, indicating strong initial plasma instability.
- **Moderate Anisotropy (Tanh = 6, 4)**: Lower initial growth rates, with more gradual decay, showing less instability compared to higher anisotropy.

- **Low Anisotropy (Tanh = 2)**: Minimal growth rate, suggesting near stability from the start.

plasma growth rate, temperature anisotropy, and the kappa distribution, showing how higher anisotropy amplifies growth rates but quickly stabilizes as the system moves toward a more thermal state with higher κ_p.

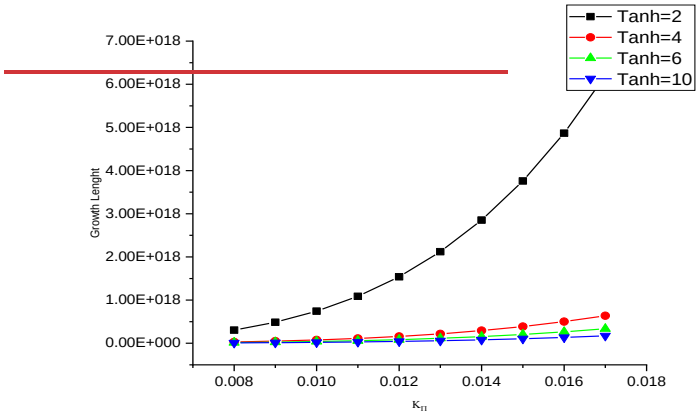

Fig. 4 Variation of growth length Lg versus wave vector $\mathbf{K_H}$ (cm^{-1}) for varying values of the Hydrogen ion Temperature Anisotropy at κ_p=2

The graph 4 indicates that as the wave vector increases, the growth length becomes larger, implying that shorter wavelength waves experience faster growth or stronger instability. The temperature anisotropy (Tanh), which reflects differences in temperature along different directions in the plasma, plays a secondary role in modulating the growth length. While its influence is more apparent at higher wave vectors, the dominant factor driving the growth length is the wave vector itself. Temperature anisotropy adds a secondary effect, especially at high wave vectors, where higher anisotropy (Tanh = 10) leads to slightly larger growth lengths compared to lower anisotropies.

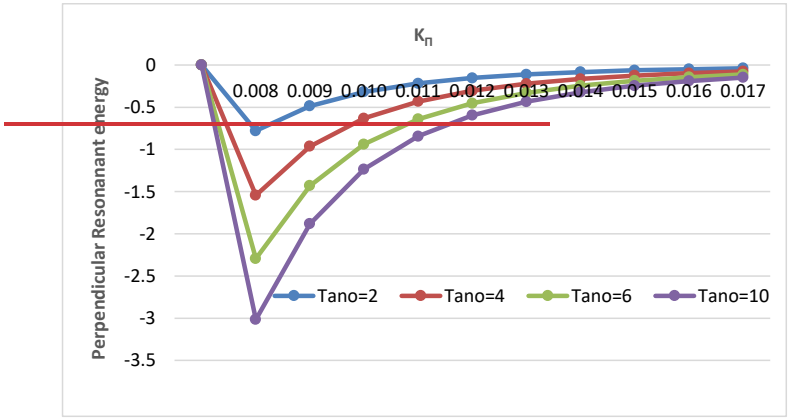

Fig. 5 Variation of the perpendicular resonant energy $W_{\perp}$ erg cm^{-1}versus the wave vector K_{Π} (cm^{-1}) for varying values of the Oxygen ion Temperature Anisotropy at κ_p=2

In figure 5 In the context of oxygen ions, the temperature anisotropy refers to the difference between the temperature in The directions parallel and perpendicular relative to the magnetic field. The sharp decrease in resonant energy with increasing κ_{π}, followed by a recovery, could imply a dynamic interaction between ions and magnetic fields. Higher anisotropy seems to enhance energy loss at lower κ_{π} , but this effect diminishes as κ_{π} increases.this graph highlights how perpendicular resonant energy is influenced by both the temperature anisotropy and the parameter κ_{π} . Higher temperature anisotropy results in a more pronounced initial energy loss, but the energy converges to similar values for all anisotropies as κ_{π} increases.

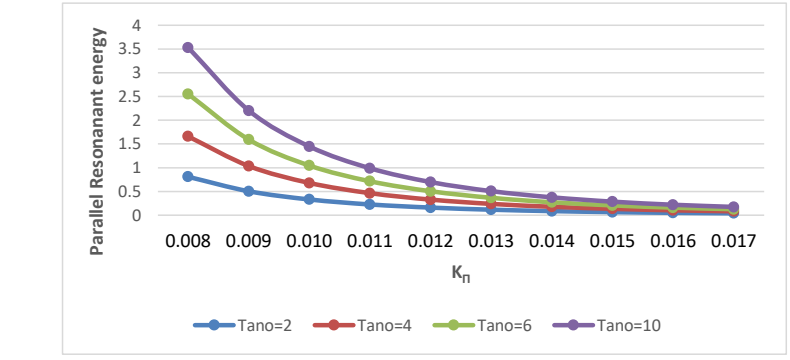

Fig. 6 Variation of parallel resonant energy W_{Π} erg cm^{-1} versus wave vector K_{Π} (cm^{-1}) for varying values of the Oxygen ion Temperature Anisotropy at κ_p=2 .

In figure 6 graph, the oxygen temperature anisotropy influences the behavior of parallel resonant energy similarly to how it affects perpendicular resonant energy. The larger the temperature anisotropy, the more pronounced the initial parallel resonant energy. However, as κ_n increases, the resonant energy decreases for all Tano values, indicating that higher values of κ_n diminish the energy differences caused by anisotropy.The sharper drop in parallel resonant energy for higher Tano values reflects the increased energy loss due to stronger anisotropy at lower κ_n . The gradual convergence of all curves at higher κ_n suggests that for large enough κ_n, anisotropy becomes less important in determining the parallel resonant energy.

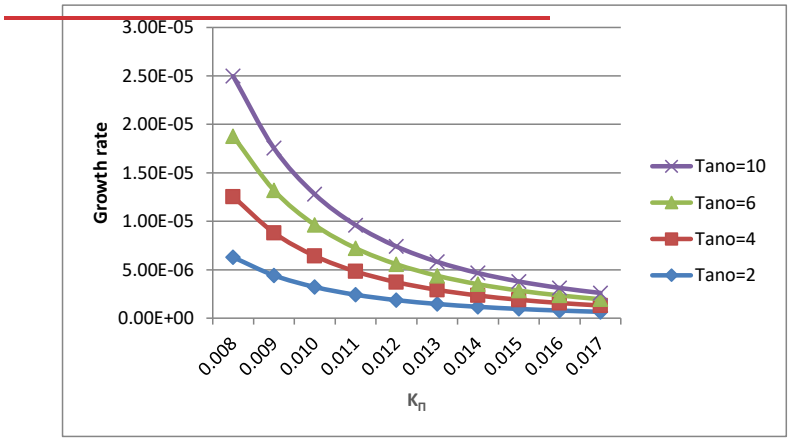

Fig. 7 Variation of growth rate (γ/ω) versus wave vector $\mathbf{K_{II}}$ (cm^{-1}) for varying values of the Oxygen ion Temperature Anisotropy at κ_p=2

In figure 7 graph For lower values of κ_n the difference in growth rates among different Temperature anisotropy in oxygen values is more pronounced, with Tano = 10 being significantly higher.As κ_n increases, the growth rates converge, and the differences between Temperature anisotropy values become less noticeable.: Higher Temperature anisotropy in oxygen values (representing some physical or operational parameter) lead to higher growth rates initially, but all curves eventually decline towards zero as κ_n increases, suggesting a diminishing effect of κ_n on growth rate regardless of Tano.

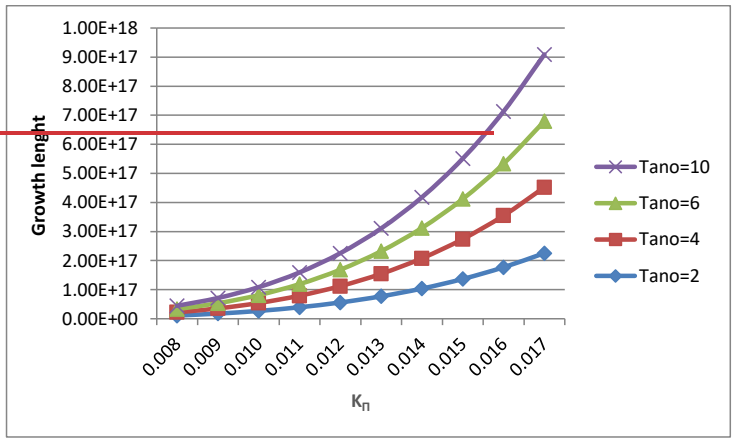

Fig. 8 Variation of growth length Lg versus wave vector K_{π} (cm^{-1})for varying values of the Oxygen ion Temperature Anisotropy at κ_p=2

The graph 8 likely represents how growth length increases as κ_{π} increases. Temperature anisotropy in oxygen plays a critical role in determining how fast or slow this growth occurs. Growth length increases exponentially with κ_{π}, and this effect is amplified by higher temperature anisotropy. Higher anisotropy values lead to a more rapid rise in growth length, especially at higher κ_{π} .The effect of anisotropy is more pronounced at higher values of κ_{π}, where the curves diverge significantly, showing that anisotropy strongly influences growth processes in such conditions.

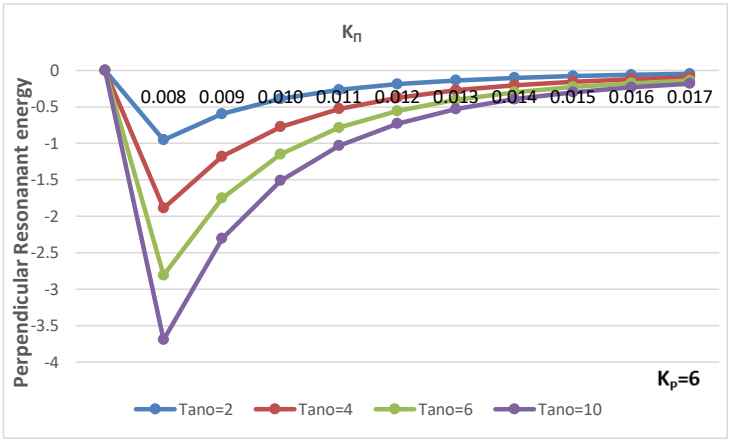

Fig. 9 Variation of the perpendicular resonant energy $W_{\perp}$ erg cm^{-1}versus the wave vector K_{π} (cm^{-1}) for varying values of the Oxygen ion Temperature Anisotropy at κ_p=6

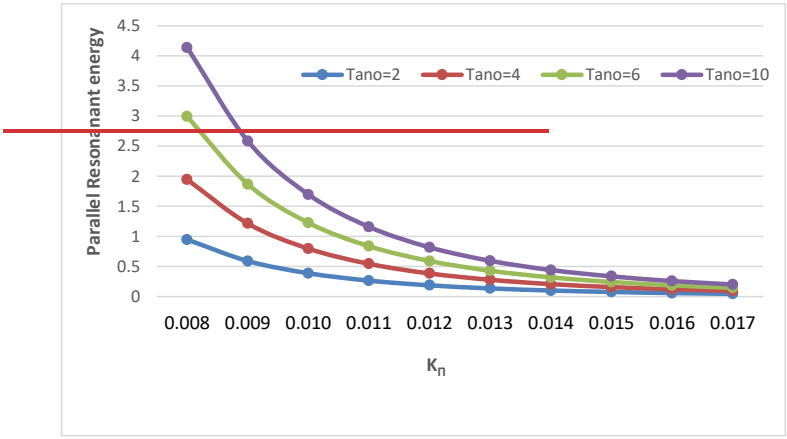

Fig. 10 Variation of parallel resonant energy W_{II} erg cm^{-1} versus wave vector K_{II} (cm^{-1}) for varying values of the Oxygen ion Temperature Anisotropy at κ_p=6 .

In figure 9 and 10 graph The perpendicular energy experiences a steep decline at the lowest κ_π values, particularly for higher Tano values, before gradually increasing towards zero as κ_π rises. This indicates a strong initial impact of anisotropy that diminishes with increasing κ_π.In contrast, the parallel resonant energy starts high and decreases steadily with κ_π. Higher Tano levels result in higher initial energy values, but similar to the perpendicular energy, all values converge towards zero as κ_π increases. The analysis reveals that oxygen temperature anisotropy significantly alters resonant energy states at low κ_π , enhancing both perpendicular and parallel energies in different ways. However, as κ_π increases, the system stabilizes, and the influence of anisotropy diminishes, leading to near-uniform energy levels regardless of the anisotropy magnitude. This behaviour highlights the complex interplay between anisotropy and κ_π in shaping energy dynamics

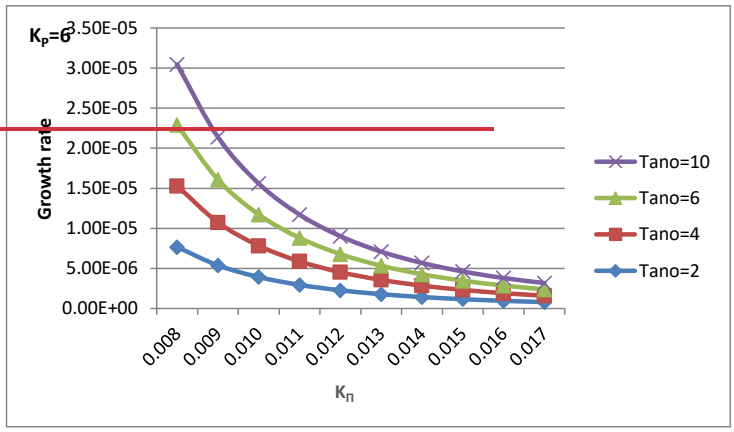

Fig. 11 Variation of growth rate (γ/ω) versus wave vector $K_п$ (cm^{-1}) for varying values of the Oxygen ion Temperature Anisotropy at κ_p=6

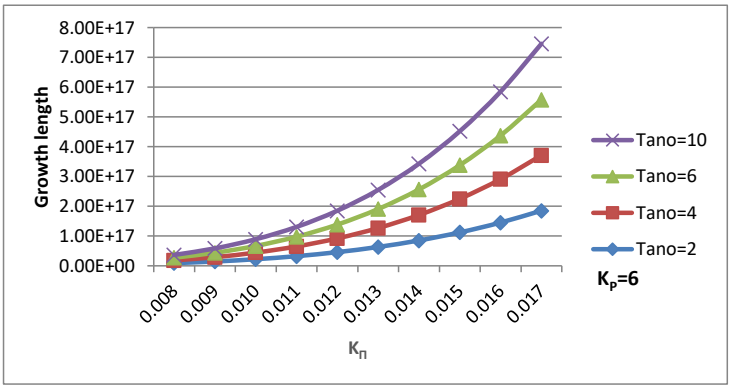

Fig. 12 Variation of growth length Lg versus wave vector $K_п$ (cm^{-1}) for varying values of the Oxygen ion Temperature Anisotropy at κ_p=6

The two graphs 11 and 12 illustrate the influence of temperature anisotropy (Tano) on growth rate and growth length as functions of $\kappa_п$, with a fixed κ_p = 6. In the 11 graphs, showing the growth rate versus $\kappa_п$, a clear trend emerges where the growth rate decreases as $\kappa_п$ increases, regardless of the Tano value. Higher Tano values, such as Tano=10, lead to significantly higher growth rates compared to lower values like Tano=2. This indicates that temperature anisotropy enhances the growth rate, particularly at lower $\kappa_п$ values. However, as $\kappa_п$ increases, the growth rates of different Tano levels converge, suggesting that the impact of Tano diminishes at higher $\kappa_п$ values.

~~In the 12 graph, which depicts growth length versus κ_π, the opposite trend is observed: growth length increases with κ_π for all Tano values. Higher Tano values correspond to much larger growth lengths, emphasizing the strong effect of temperature anisotropy on this metric. The separation between the growth length curves becomes more pronounced as κ_π increases, with higher Tano values resulting in significantly greater growth lengths. This suggests that while the impact of Tano on growth rate lessens with increasing κ_π, its influence on growth length remains substantial.~~

~~Overall, the combined analysis highlights the critical role of temperature anisotropy in determining growth dynamics. Higher Tano values enhance both growth rate and growth length. This interplay suggests that while κ_p inversely affects growth rate and positively influences growth length, the extent of these effects is strongly modulated by the degree of temperature anisotropy.~~

9. Summary of Results and Discussion

This is a comprehensive analysis of EMIC wave dynamics, covering perpendicular and parallel resonant energies, growth rates, and growth lengths, all influenced by temperature anisotropies and the kappa parameter. Here's a summary of the key results and a discussion of their vital roles:

1. Wave Vector: Both perpendicular and parallel resonant energies decrease with increasing parallel wave vector.
2. Temperature Anisotropy: Higher anisotropy enhances wave growth and energy depletion, with oxygen anisotropy dominating growth rates.
3. Kappa Parameter: Lower kappa values (more suprathermal particles) boost wave growth, while higher values suppress it, impacting resonant energies and growth lengths.
4. Ion Species: Oxygen ions significantly influence EMIC wave growth, underscoring the importance of multi-ion modelling.

Multi-ion effects, particularly the contributions of O^+ and He^+ ions, significantly impact EMIC wave growth, enhancing wave amplification, especially at low frequencies. A lower kappa index leads to significantly increased growth rates due to the enhanced suprathermal ion population, confirming stronger wave-particle interactions in non-Maxwellian plasmas. Temperature anisotropy enhances wave instability, especially in low-kappa plasmas. The observed differences in wave growth between the auroral region and

Formatted: Font: (Default) Times New Roman, 12 pt, Bold, Complex Script Font: Times New Roman, 12 pt, Bold

Formatted: Font: (Default) Times New Roman, 12 pt, Complex Script Font: Times New Roman, 12 pt

Formatted: List Paragraph, Numbered + Level: 1 + Numbering Style: 1, 2, 3, … + Start at: 1 + Alignment: Left + Aligned at: 0.32 cm + Indent at: 0.95 cm

Formatted: Justified, Space Before: 0 pt, After: 0 pt

plasmapause have important implications for energy dissipation and particle scattering. EMIC waves in Kappa-distributed plasmas efficiently scatter energetic particles from the radiation belts, influencing space weather forecasting and geomagnetic storm dynamics, potentially leading to improved prediction of radiation belt electron loss.

10.Conclusion~~:~~

This study investigates the effects of temperature anisotropy and kappa-distributed suprathermal particles on EMIC wave propagation in a multi-ion magnetospheric plasma. Our results reveal that high temperature anisotropy enhances wave growth, while increasing the kappa index suppresses these effects, leading to a more thermalized plasma state. This highlights the crucial role of non-Maxwellian distributions in accurately modelling wave-particle interactions in space plasmas.

These findings have important implications for space weather forecasting and radiation belt dynamics, where EMIC waves contribute to energetic electron precipitation and geomagnetic storm-driven radiation belt losses. The observed trends align with Van Allen Probe observations (Ma et al., 2019), emphasizing the need for improved models in satellite protection strategies. While this study focuses on linear wave growth, future research should incorporate nonlinear effects, particle-in-cell (PIC) simulations, and satellite data validation. Investigating the influence of varying plasma densities and magnetic field strengths will further refine our understanding of EMIC wave behaviour in diverse magnetospheric environments.

Competing interests

The contact author has declared that none of the authors has any competing interests.

~~This study has explored the impact of temperature anisotropy and the Kappa distribution function on the propagation and characteristics of electromagnetic ion cyclotron (EMIC) waves in a multi-ion magneto-plasma environment. By incorporating the effects of~~

Formatted: Font: (Default) Times New Roman, 14 pt, Bold, Complex Script Font: Times New Roman, 14 pt, Bold

Formatted: List Paragraph, Numbered + Level: 1 + Numbering Style: 1, 2, 3, … + Start at: 1 + Alignment: Left + Aligned at: 0.32 cm + Indent at: 0.95 cm

~~anisotropic thermal conditions and non-Maxwellian particle distributions, the research provides a deeper understanding of how these factors alter wave dynamics, including dispersion relations, growth rates, and energy states. Our findings reveal significant deviations from classical models, emphasizing the necessity to account for both temperature anisotropy and suprathermal particles for accurate modeling of wave behavior in realistic space and laboratory plasmas.~~

~~The results demonstrate that high levels of temperature anisotropy lead to notable changes in wave characteristics, such as enhanced growth rates and altered resonant energy patterns. As the Kappa distribution index increases, these effects tend to diminish, indicating that the influence of anisotropy becomes less pronounced in more thermalized systems. This nuanced interaction between anisotropy and the Kappa distribution highlights the complexity of plasma wave dynamics, especially in environments like the Earth's magnetosphere and other astrophysical contexts where multi-ion interactions and non-equilibrium conditions prevail.~~

~~Overall, this study enhances the overall comprehension of space plasma physics and has potential applications in predicting wave behavior in the Earth's magnetosphere, astrophysical plasma conditions, and controlled plasma experiments. Future research should explore these interactions under varying magnetic field strengths and other plasma parameters to further refine theoretical models and enhance the predictive capabilities for space weather phenomena.~~

Reference

Ahirwar, G. and Meda, R.: Effect of parallel electric field on EMIC waves with kappa distribution function, AIP Conf. Proc., 2224, 040018, https://doi.org/10.1063/5.0000681, 2020.

Ahirwar, G., Varma, P., and Tiwari, M. S.: Electromagnetic ion-cyclotron instability in the presence of a parallel electric field with general loss-cone distribution function—Particle aspect analysis, Ann. Geophys., 24, 1919–1929, https://doi.org/10.5194/angeo-24-1919-2006, 2006.

Cattaert, T., Hellberg, M. A., and Mace, R. L.: Oblique propagation of electromagnetic waves in a kappa-Maxwellian plasma, Phys. Plasmas, 14, 082111, https://doi.org/10.1063/1.2766647, 2007.

Cornwall, J. M.: Cyclotron instabilities and electromagnetic emission in the ultra-low frequency and very low frequency ranges, J. Geophys. Res., 70, 61–69, https://doi.org/10.1029/JZ070i001p00061, 1965.

Erlandson, R. E., Aggson, T. L., Hogey, W. R., and Slavin, J. A.: Simultaneous observations of subauroral electron temperature enhancements and electromagnetic ion cyclotron waves, Geophys. Res. Lett., 20, 1723–1726, https://doi.org/10.1029/93gl01975, 1993.

Gary, S. P. and Lee, M. A.: The ion cyclotron anisotropy instability and the inverse correlation between proton anisotropy and proton beta, J. Geophys. Res. Space Phys., 99, 11297–11302, https://doi.org/10.1029/94JA00253, 1994.

Hellberg, M. A. and Mace, R. L.: Generalized plasma dispersion function for a plasma with a kappa-Maxwellian velocity distribution, Phys. Plasmas, 9, 1495–1504, https://doi.org/10.1063/1.1462636, 2002.

Hellinger, P. and Matsumoto, H.: New kinetic instability: Oblique Alfvén fire hose, J. Geophys. Res. Space Phys., 105, 10519–10526, https://doi.org/10.1029/1999JA000297, 2000.

Formatted: Indent: First line: 2 cm

Kennel, C. F. and Petschek, H. E.: Limit on stably trapped particle fluxes, J. Geophys. Res., 71, 1–28, https://doi.org/10.1029/JZ071i001p00001, 1966.

Klimas, A. J., Vassiliadis, D., and Baker, D. N.: Dst index prediction using data-derived analogues of the magnetospheric dynamics, J. Geophys. Res. Space Phys., 103, 20435–20447, https://doi.org/10.1029/98JA01559, 1998.

Kozyra, J. U., Shelley, E. G., Comfort, R. H., Brace, L. H., Cravens, T. E., and Nagy, A. F.: The role of ring current O+ in the formation of stable auroral red arcs, J. Geophys. Res., 92, 7487–7502, https://doi.org/10.1029/JA092iA07p07487, 1987.

Lazar, M. and Schlickeiser, R.: Covariant kinetic theory for nonlinear plasma waves interaction, J. Plasma Phys., 72, 711–720, https://doi.org/10.1017/S0022377805004253, 2006.

Lazar, M., Schlickeiser, R., and Shukla, P. K.: Cumulative effect of the filamentation and Weibel instabilities in counterstreaming thermal plasmas, Phys. Plasmas, 13, 102107, https://doi.org/10.1063/1.2357047, 2006.

Livadiotis, G.: Kappa Distributions: Theory and Applications in Plasmas, Elsevier, 1st Edn., 380 pp., ISBN 9780128046388, 2017.

Lazar, M.: The electromagnetic ion-cyclotron instability in bi-Kappa distributed plasmas, Astron. Astrophys., 547, A94, https://doi.org/10.1051/0004-6361/201219861, 2012.

Ma, Q., Li, W., Yue, C., Thorne, R. M., Bortnik, J., Kletzing, C. A., Kurth, W. S., Hospodarsky, G. B., Reeves, G. D., and Spence, H. E.: Ion Heating by Electromagnetic Ion Cyclotron Waves and Magnetosonic Waves in the Earth's Inner Magnetosphere, Geophys. Res. Lett., 46, 6258–6267, https://doi.org/10.1029/2019GL083513, 2019.

Meda, R. and Ahirwar, G.: Effect of kappa distribution function on EMIC waves in cold magnetized plasma by particle aspect analysis, J. Emerg. Technol. Innov. Res., 8(8), 410, https://www.jetir.org, 2021.

Omura, Y., Pickett, J., Grison, B., Santolik, O., Dandouras, I., Engebretson, M., Decreau, P. M. E., and Masson, A.: Theory and observation of electromagnetic ion cyclotron triggered emissions in the magnetosphere, J. Geophys. Res., 115, A07234, https://doi.org/10.1029/2010JA015300, 2010.

Patel, S., Varma, P., and Tiwari, M. S.: Electromagnetic ion cyclotron waves in multi-ions hot anisotropic plasma in auroral acceleration region-particle aspect approach, Earth Moon Planets, 109, 29–41, https://doi.org/10.1007/s11038-012-9400-4, 2012.

Pierrard, V. and Lazar, M.: Kappa Distributions: Theory and Applications in Space Plasmas, Sol. Phys., 267, 153–174, https://doi.org/10.1007/s11207-010-9640-2, 2010.

Sugiyama, H., Singh, S., Omura, Y., Shoji, M., Nunn, D., and Summers, D.: Electromagnetic ion cyclotron waves in the Earth's magnetosphere with a kappa-Maxwellian particle distribution, J. Geophys. Res. Space Phys., 120, 8426–8439, https://doi.org/10.1002/2015JA021346, 2015.

Summers, D. and Thorne, R. M.: The modified plasma dispersion function, Phys. Fluids B Plasma Phys., 3(7), 1835–1847, https://doi.org/10.1063/1.859653, 1991.

Usanova M. E., Drozdov A., Orlova K., Mann I. R., Shprits Y., Robertson M. T., Turner D. L., Milling D. K., Kale A., Baker D. N., Thaller S. A., Reeves G. D., Spence H. E., Kletzing C., Wygant J.:Effect of EMIC waves on relativistic and ultrarelativistic electron populations: Ground-based and Van Allen Probes observations, *Geophys. Res. Lett.*, **41**, 1375–1381, https://doi.org/10.1002/2013GL059024, 2014.

Vasyliunas, V. M.: Survey of low-energy electrons in the evening sector of the magnetosphere with OGO 1 and OGO 3, J. Geophys. Res., 73(9), 2839, https://doi.org/10.1029/JA073i009p02839, 1968.

Xiao, F., Zhou, Q., He, H., Zheng, H., and Wang, S.: Electromagnetic ion cyclotron waves instability threshold condition of suprathermal protons by kappa distribution, J. Geophys. Res., 112, A07219, https://doi.org/10.1029/2006JA012050, 2007.

Xue, S., Thorne, R. M., and Summers, D.: Electromagnetic ion-cyclotron instability in space plasmas, J. Geophys. Res., 98(A10), 17475–17484, https://doi.org/10.1029/93JA00790, 1993.

Xue, S., Thorne, R. M., and Summers, D.: Growth and damping of oblique electromagnetic ion cyclotron waves in the Earth's magnetosphere, J. Geophys. Res., 101(A7), 15457–15466, https://doi.org/10.1029/96JA01088, 1996 a.

Xue, S., Thorne, R. M., and Summers, D.: Parametric study of electromagnetic ion cyclotron instability in the Earth's magnetosphere, J. Geophys. Res. Space Phys., 101(A7), 15467–15474, https://doi.org/10.1029/96JA01087, 1996 b.

Yan, G., Shen, C., Liu, Z., and others: Solar wind transport into the magnetosphere caused by magnetic reconnection at high latitude magnetopause during northward IMF: Cluster-DSP conjunction observations, Sci. China Ser. E Technol. Sci., 51, 1677–1684, https://doi.org/10.1007/s11431-008-0260-0, 2008.

~~1. Meda, R., & Ahirwar, G. (2021). Investigating electromagnetic ion cyclotron wave propagation in multi-ion plasmas. JETIR, 8(8), 1-6.~~

~~2. Ahirwar, G., Varma, P., & Tiwari, M. S. (2010). Ion cyclotron resonance in magnetospheric plasmas. Indian Journal of Pure & Applied Physics, 48, 334-342.~~

3. Ahirwar, G., Varma, P., & Tiwari, M. S. (2006). Electromagnetic wave propagation in magnetospheric plasmas. Indian Journal of Physics, 80, 1179-1187.
4. Anderson, B. J., & Williams, D. J. (1999). The electromagnetic ion cyclotron wave and its interaction with the magnetosphere. Space Science Reviews, 89(1-2), 253-268.
5. Chen, L. J., & Hasegawa, A. (1974). The influence of temperature anisotropy on the properties of EMIC waves. Journal of Geophysical Research, 79(19), 2894-2904.
6. Del Sarto, D., Pegoraro, F., & D'Angelo, R. (2011). Wave propagation in non-Maxwellian plasmas. Physics of Plasmas, 18(10), 102104.
7. Hellinger, P., & Matsumoto, Y. (2000). The effect of temperature anisotropy on ion cyclotron waves in a multi ion plasma. Journal of Geophysical Research, 105(A10), 23139-23148.
8. Kennel, C. F., & Petschek, H. E. (1966). Limit on stably trapped particle fluxes. Journal of Geophysical Research, 71(1), 1-28.
9. Pierrard, V., & Lazar, M. (2010). Kappa distributions: A review. Nonlinear Processes in Geophysics, 17(3), 209-220.
10. Scholer, M. (1988). The effect of temperature anisotropy on the growth of electromagnetic ion cyclotron waves. Journal of Geophysical Research, 93(A8), 8753-8764.
11. Vasyliunas, V. M. (1968). Theoretical models of magnetospheric convection. Journal of Geophysical Research, 73(21), 7466-7481.
12. Zhang, J., & Chen, L. (2003). Temperature anisotropy effects on the stability of ion cyclotron waves. Physics of Plasmas, 10(4), 1148-1156.
13. Ahirwar, G., Varma, P., & Tiwari, M. S. (2006). Ion cyclotron instability in magnetospheric plasmas. Annales Geophysicae, 24, 1919-1932.
14. Meda, R., & Ahirwar, G. (2022). Study of EMIC waves in space plasmas. International Journal of Scientific Development and Research, 7(9), 1-7.
15. Sharma, J., & Ahirwar, G. (2013). Study on EMIC waves in multi ions around the plasmapause region. Research Journal of Physical Sciences, 1(3), 26-29.
16. Summers, D., & Thorne, R. M. (2003). Electromagnetic ion cyclotron instability in space plasmas. Journal of Geophysical Research, 108(A4), 1143. https://doi.org/10.1029/2002JA009489
17. Gamayunov, K. V., Khazanov, G. V., Liemohn, M. W., Fok, M. C., & Ridley, A. J. (2009). Self-consistent magnetosphere-ionosphere coupling model. Journal of Geophysical Research: Space Physics, 114, A03221.

18. Kennel, C. F., & Petschek, H. E. (1966). Limit on stably trapped particle fluxes. Journal of Geophysical Research, 71(1), 1-28.
19. Erlandson, R. E., & Ukhorskiy, A. Y. (2001). Interactions between electromagnetic ion cyclotron waves and ring current ions. Journal of Geophysical Research: Space Physics, 106(A5), 3883-3890.
20. Anderson, B. J., Erlandson, R. E., & Zanetti, L. J. (1992). A statistical study of Pc 1-2 magnetic pulsations in the equatorial magnetosphere: 1. Equatorial occurrence distributions. Journal of Geophysical Research: Space Physics, 97(A3), 3075-3088.
21. Gurgiolo, C., Sandel, B. R., Perez, J. D., Mitchell, D. G., Pollock, C. J., & Larsen, B. A. (2005). MHD waves in the outer magnetosphere. Journal of Geophysical Research: Space Physics, 110, A12217.
22. Mozer, F. S., Carlson, C. W., & Hudson, M. K. (1977). Electromagnetic ion cyclotron waves and their interactions with the magnetosphere. Physical Review Letters, 38(6), 292-295.
23. Temerin, M., Cerny, K., Lotko, W., & Mozer, F. S. (1982). The role of Alfvén waves in auroral particle acceleration. Physical Review Letters, 48(18), 1175-1178.
24. Song, Y., & Lysak, R. L. (2006). Alfvén waves and their role in the magnetosphere-ionosphere coupling. Physical Review Letters, 96, 145002.
25. Lund, E. J., Mobius, E., Carlson, C. W., et al. (2000). Investigating wave propagation and reflection in the magnetosphere. Journal of Atmospheric and Solar-Terrestrial Physics, 62(4), 467-476.
26. Khazanov, G. V., Gamayunov, K. V., Gallagher, D. L., & Kozyra, J. U. (2006). Electromagnetic ion cyclotron waves and their effects in the magnetosphere. Journal of Geophysical Research: Space Physics, 111, A10202. https://doi.org/10.1029/2006JA011833
27. Lund, E. J., Mobius, E., Klumpar, D. M., et al. (1999). Observations of plasma wave activity in the Earth's magnetosphere. Advances in Space Research, 23(10), 1721-1726.
28. Varma, P., Ahirwar, G., & Tiwari, M. S. (2008). Electromagnetic ion cyclotron waves and their interaction with multi ion plasmas. Planetary and Space Science, 56(8), 1023-1031.
29. Vasyliunas, V. M. (1968). A survey of low-energy electrons in the evening sector of the magnetosphere with OGO 1 and OGO 3. Journal of Geophysical Research, 73(9), 2839-2884. https://doi.org/10.1029/JA073i009p02839

30. Pierrard, V., & Lazar, M. (2010). Kappa distributions: Theory and applications in space plasmas. Solar Physics, 267(1), 153-174. https://doi.org/10.1007/s11207-010-9640-2
31. Gary, S. P., & Lee, M. A. (1994). The ion cyclotron anisotropy instability and the inverse correlation between proton anisotropy and proton beta. Journal of Geophysical Research: Space Physics, 99(A6), 11297-11302. https://doi.org/10.1029/94JA00253
32. Hellinger, P., Trávníček, P. M., Kasper, J. C., & Lazarus, A. J. (2006). Solar wind proton temperature anisotropy: Linear theory and WIND/SWE observations. Geophysical Research Letters, 33(9). https://doi.org/10.1029/2006GL025925
33. Baumjohann, W., & Treumann, R. A. (1997). Basic Space Plasma Physics. Imperial College Press.
34. Schindler, K. (2007). Physics of Space Plasma Activity. Cambridge University Press.
35. Cornwall, J. M., & Schulz, M. (1971). Theoretical investigation of ion cyclotron resonance. Journal of Geophysical Research, 76(31), 7791-7800.
36.1. Upadhyay, A., Kakad, B., Kakad, A., Omura, Y., & Sinha, A. K. (2019). Electromagnetic ion cyclotron waves and their impact on plasma. Proceedings of URSI AP-RASC, pp. 1-1. https://doi.org/10